Geopersia 2026, 16(1): 89-113
DOI: 10.22059/geope.2025.395854.648821

RESEARCH PAPER

# Using SFA and GMPI methods for geochemical exploration of buried porphyry copper deposits, case study: Janja copper-gold deposit, SE Iran

**Masoud Esmailzadeh, Ali Imamalipour ***

Department of Mining Engineering, Urmia University, Urmia, Iran

Received: 23 May 2025, Revised: 03 August 2025, Accepted: 17 August 2025

**Abstract**
The Janja Porphyry Copper-Gold Deposit, situated in the Zabol–Zahedan–Saravan subzone of Eastern Iran, is obscured by a thick alluvial cover, which complicates exploration. This study investigates the geochemical distribution of elements in surface cover to delineate anomaly patterns associated with concealed mineralization. A total of 153 stream sediment samples and 16,300 drill core samples from 74 boreholes (38 in overburden, 36 in exposed bedrock) were analyzed using ICP-MS and Fire Assay techniques. Centered Log-Ratio (CLR) transformation, Staged Factor Analysis (SFA), and Geochemical Mineralization Prediction Index (GMPI) delineate anomaly patterns associated with concealed porphyry and vein-type mineralization. Results show that the concentrations of elements Ag, As, Cd, Mo, Pb, S, Sb, and Zn have increased in the overburden (up to five times Clarke values), with Cu (1,211.53 ppm) and Au (0.1 ppm) enriched in hypogene diorite (2,561.4 ppm Cu, 0.15 ppm Au). SFA identified three elemental groups, including lithogenic (Al, Fe, Mn), mineralization-related (Cu, Pb, Zn, Ag), and broadly dispersed elements (Mo, As, S). Anomalous concentrations of Ag, Mo, Cd, and S elements in overburden serve as key indicators for concealed deposits. This CLR-SFA-GMPI approach mitigates closure effects, enhances anomaly detection, and offers a scalable strategy for exploring porphyry Cu deposits in arid covered terrains within global porphyry belts.

**Keywords:** Geochemical Exploration, Janja Porphyry Cu Deposit, Overburden, GMPI, SFA.

## Introduction

Porphyry deposits rank among the most critical targets in mineral resource assessment due to their substantial contributions to global copper, gold, and molybdenum production(Cooke et al., 2014; Lowell & Guilbert, 1970; Sillitoe, 2010). These deposits are frequently affected by erosion and weathering, often remaining concealed beneath alluvial, colluvial, or weathered materials, which complicates their detection and increases exploration costs (Anand et al., 2016; Butt et al., 2000; Moradpouri et al., 2023). The global decline in the discovery of economic deposits, coupled with rising demand for base and precious metals, underscores the urgent need for innovative exploration techniques (Hagemann et al., 2016; Kelley et al., 2004). Many mineral resources are estimated to remain undiscovered under thick sedimentary cover, where surface conditions—both lithological and non-lithological—modulate geochemical signals from underlying mineralization (Anand et al., 2014; Butt et al., 2000). Consequently, extensive research and exploration efforts have focused on these challenging environments (Hou et al., 2004; Sillitoe, 2010).

Exploration efforts increasingly target deeper deposits in so-called "brownfields," as greenfield exploration is typically costlier and riskier (Hagemann et al., 2016). Conducting

* Corresponding author e-mail: a.imamalipour@urmia.ac.ir

surveys near known mines enhances the likelihood of uncovering hidden deposits. Detecting deep mineralization requires integrating geological, geochemical, geophysical, and three-dimensional spatial analysis methods to model and assess subsurface mineral systems (Fallara et al., 2006; Hosseini-Dinani & Aftabi, 2016; Porwal & Carranza, 2015; J. Wang et al., 2017; M. Wang et al., 2017).

The primary goal of regional-scale geochemical exploration is to identify anomalies and correlate them with mineralized zones through stream sediment analysis (Esmaeiloghli, Lima, et al., 2024; Esmaeiloghli, Tabatabaei, et al., 2024; Ghasemzadeh et al., 2019; Saremi et al., 2023). These sediments, formed by the erosion of upstream rocks within drainage basins, provide insights into mineralization and lithological characteristics (Shahrestani & Mokhtari, 2017a, 2017b; Shahrestani, Mokhtari, & Alipour-Asll, 2019; Shahrestani, Mokhtari, Carranza, et al., 2019). However, factors such as topography, slope, lithology, and faulting affect these data nonlinearly, posing challenges for interpretation (Yousefi et al., 2013). Advances in data mining, statistical, and intelligent methods have facilitated the extraction of complex patterns (Zuo, 2017; Zuo et al., 2021). Spatial geochemical data are essential for delineating mineralization boundaries and understanding element transport and dispersion (Ayari et al., 2022; Bigdeli et al., 2023; Hajihosseinlou et al., 2024a, 2024b). Geochemical maps, by highlighting anomalies, assist in identifying deposit types and supporting Mineral Prospectivity Mapping (MPM) (Barak et al., 2024; Barak et al., 2021; Hajihosseinlou et al., 2023, 2024a, 2024b; Mirzabozorg & Abedi, 2023; Saremi et al., 2025; Saremi, Hoseinzade, et al., 2024; Saremi, Maghsoudi, et al., 2024). Multivariate analysis, in particular, offers effective tools for exploring covered terrains by detecting elemental anomalies and dispersion patterns in surface sediments (Ghasemzadeh et al., 2022; Yousefi et al., 2019).

Recent advancements in processing compositional data, such as the Centered Log-Ratio (CLR) transformation to address closure effects and Staged Factor Analysis (SFA) to reduce noise and enhance anomalies, have significantly improved exploration accuracy and efficiency (Yousefi et al., 2014; Zuo et al., 2021). Understanding the distribution patterns of geochemical elements is a fundamental step in assessing future geological and anthropogenic changes and interpreting past processes (Batanova & Sobolev, 2000; Carranza, 2008; Reimann et al., 2011; Wang & Zuo, 2024). Geochemical data from diverse samples—such as soil, stream sediments, and bedrock—reflect a wide range of geological and chemical processes (Grunsky & de Caritat, 2019; Grunsky, 2010; Grunsky et al., 2009). Analyzing background levels and spatial distributions of these elements plays a key role in pinpointing potential exploration targets (Cheng, 1996). However, their distribution results from complex, long-term interactions between primary and secondary geological processes, as well as human activities (Macklin et al., 1994; Spadoni, 2006; Wang et al., 2020). Geochemical data analysis demands a systematic approach to process and interpret high-dimensional multivariate data, providing a reliable foundation for exploration. Common challenges include the closure effect, selecting appropriate multivariate methods, and identifying anomalies (Grunsky, 2010; Tolosana-Delgado & Van den Boogaart, 2013). Thus, developing a comprehensive framework to address these issues is essential for a scientifically robust analysis.

This study provides valuable insights into the behavior of elements within semi-transitional and transitional alluvial covers under arid conditions through the detailed identification of geochemical patterns in the Janja porphyry copper deposit. The Janja porphyry copper deposit, located in the Zabol-Zahedan-Saravan subzone of Eastern Iran's structural belt, exemplifies a concealed mineral system. It formed due to the intrusion of diorite to granodiorite bodies into Late Cretaceous flysch-type rocks, with significant portions now buried beneath semi-transitional alluvial cover as a result of erosion and sedimentation processes (Camp & Griffis, 1982; Moradi et al., 2014). Previous exploration efforts in this region have achieved limited success, hindered by the limitations of conventional methods, arid desert conditions, and

complex structural features (Moradpouri et al., 2023). Nevertheless, the deposit's distinctive geochemical characteristics—especially the enrichment of key elements in the surface cover—indicate significant potential for discovering hidden resources.

This research aims to investigate the geochemical distribution of elements in the alluvial cover of the Janja area and identify indicators of concealed mineralization. It employs geochemical data from 153 stream sediment samples and 74 drillholes, utilizing advanced techniques such as the Centered Log-Ratio (CLR) transformation for data normalization, Staged Factor Analysis (SFA) for multi-element pattern analysis, and the Geochemical Mineralization Prediction Index (GMPI) for spatial anomaly mapping. This approach reveals geochemical patterns linked to porphyry and vein-type mineralization, offering a deep understanding of element behavior in arid, covered terrains and proposing an innovative framework for exploration applicable to similar porphyry belts worldwide.

The paper commences with a description of the geology and mineralization characteristics of the Janja deposit, followed by details on sampling methods, geochemical analyses, and statistical techniques. Subsequent sections present the results of univariate and multivariate analyses, including elemental distribution maps, and discuss the exploration implications of the findings along with recommendations for future research.

## Geology of the Janja Area

The Janja porphyry copper deposit lies in the Saberi region, Nimruz County, Sistan and Baluchestan Province, within the Zabol-Zahedan-Saravan subzone of Eastern Iran's structural belt. Regionally, this area is located in the western part of the Chagai magmatic arc. The Chagai arc, extending from Pakistan into Southeast Iran, is a prominent metallogenic belt renowned for its porphyry copper deposits (Mastoi et al., 2020; Perelló et al., 2008; Shah et al., 2020; Siddiqui et al., 2018; Siddiqui et al., 2017; Zürcher et al., 2019). Part of the Tethyan metallogenic belt (Hong et al., 2025; Muhammad et al., 2024; Murad et al., 2021; Zhang et al., 2024), this arc spans approximately 300 km east-west and features superimposed magmatic arcs with mineralization events from 43–37 Ma (middle-late Eocene), 24–22 Ma (early Miocene), and 18–15 Ma (middle Miocene) (Perelló et al., 2008). This complex region, with significant metallogenic potential, hosts world-class deposits like Reko Diq, Shadan, and potentially Hired (Perelló et al., 2008; Raeisi et al., 2023), linked to subduction-related magmatism and tectonic activity from the Cretaceous to Quaternary (Muhammad et al., 2024; Nicholson et al., 2010).

Positioned in the Flysch Belt between the Lut Desert and Hamun Basins, the Zabol-Zahedan-Saravan subzone adjoins the Oligocene to Middle Miocene magmatic arc (Camp and Griffis, 1982; Moradi et al., 2014). Host rocks comprise Late Cretaceous flysch (Sefidabeh Formation), including shale, sandstone, fine-grained conglomerate, and limestone interbeds, metamorphosed by diorite, quartz diorite, and granodiorite intrusions into medium- to low-temperature hornfels-skarn facies (Griffis, 1990).

Porphyry mineralization at Janja is confirmed by Miocene, U–Pb zircon ages (16.5 ± 0.5 Ma), is tied to diorite to granodiorite intrusions with porphyritic textures, comprising plagioclase, hornblende, minor quartz, and chalcopyrite. Hydrothermal alteration includes potassic, propylitic, argillic, and rare phyllic zones, associated with disseminated, veinlet, and stockwork mineralization. The mineralogy includes sulfide minerals such as pyrite, chalcopyrite, covellite, chalcocite, molybdenite and bornite; and oxide minerals including magnetite, hematite, goethite, and hydro-carbonate minerals including malachite and azurite (Rahimi et al., 2022) (Figure 1).

Much of the area is covered by Quaternary alluvium and dunes, up to 17 m thick, obscuring surface mineralization and necessitating advanced geochemical methods (IMPASCO, 2022). The landscape features rugged hornfels outcrops and gently sloping dioritic bodies, with enriched alluvial elements creating favorable conditions for studying concealed mineralization (Figure 2).

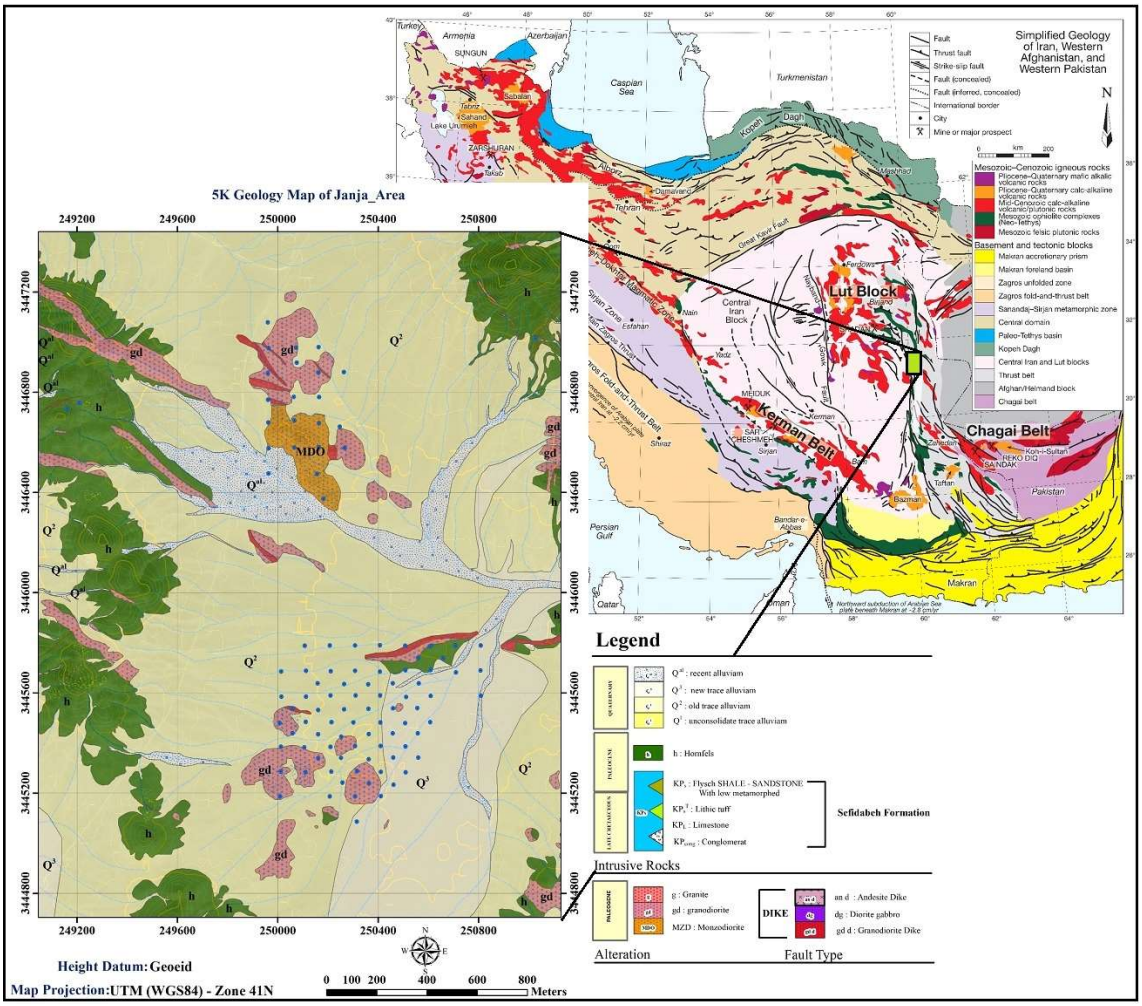


**Figure 1.** The geological map of the study area, at a scale of 1:5000, has been revised from IMPASCO (2022)

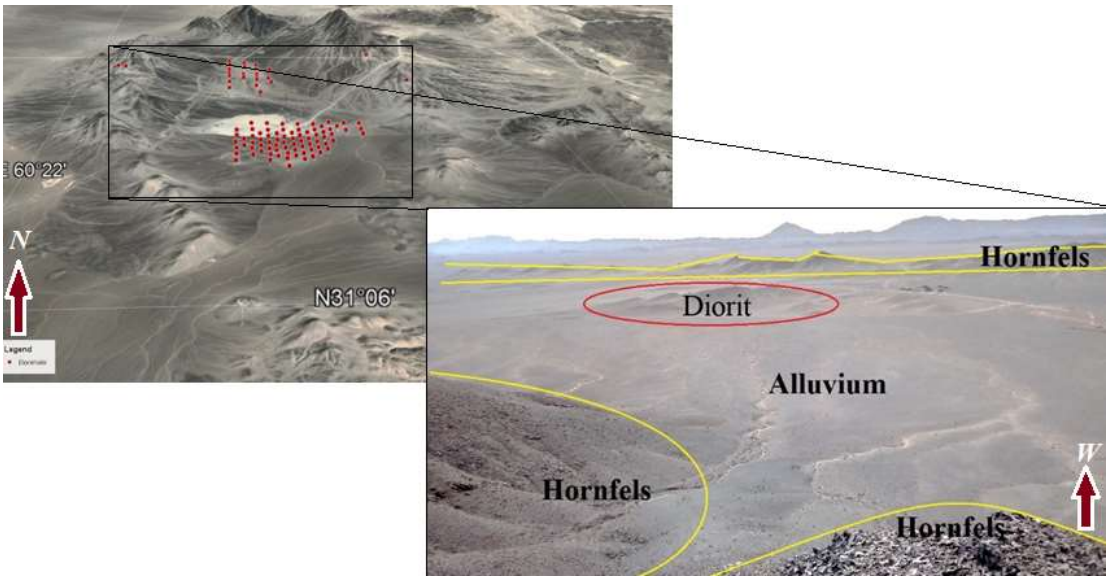


**Figure 2.** General view of the study area and drilled boreholes in the Janja area.; Rough areas indicate hornfels outcrops and gently sloping areas related to the diorite-quartz porphyry intrusion

Exploration drilling reveals a mineralized zone extending beyond 700 m, with reserves of 238 million metric tons at 0.31 wt.% Cu and 0.28 ppm Au. Polymetallic Au-Ag-Cu-Pb-Zn vein systems (1–10 m thick) along SE trending faults host galena, sphalerite, chalcopyrite, and malachite, with over 40 historical mining localities highlighting the region's potential (Olang, 2016). The central intrusion lies under alluvial cover, with exposures in the north.

## Materials and Methods

This investigation utilized geochemical data derived from 153 stream sediment samples and 16,300 drill core samples extracted from 74 boreholes across the Janja porphyry copper deposit. Stream sediment samples were systematically gathered from both active and inactive drainage systems to assess the distribution of elements within the alluvial cover. Among the 74 boreholes, 38 were positioned within the alluvial overburden, while 36 penetrated exposed bedrock zones. Drill core samples, collected from the 0–10 meter depth range in overburden boreholes, were selected to analyze elemental patterns within the semi-transitional alluvial cover. The maximum overburden thickness, measured at 17.2 meters, was recorded in borehole BH23 (IMPASCO, 2022). Sampling protocols adhered to exploration standards compliant with ISO 17025 (Figure 4).

Stream sediment samples underwent drying at 60°C, sieving to -80 mesh, and reduction to a final weight of 50 grams. Drill core samples were pulverized to <2 mm, homogenized, and reduced to 100 grams. Geochemical analysis of 19 elements (comprising Ag, Au, Al, As, Ca, Cd, Cr, Cu, Fe, Li, Mg, Mn, Mo, Ni, Pb, S, Sb, V, Zn) was conducted using ICP-MS (Agilent 7700) at the Zar Azma Laboratory. Gold analysis employed the Fire Assay method (Au-AA23, with a detection limit of 1 ppb), whereas other elements were assessed with the following detection limits: Cu (1 ppm), Ag (0.1 ppm), Mo (0.5 ppm), Zn (1 ppm), Pb (1 ppm), As (0.5 ppm), and S (10 ppm).

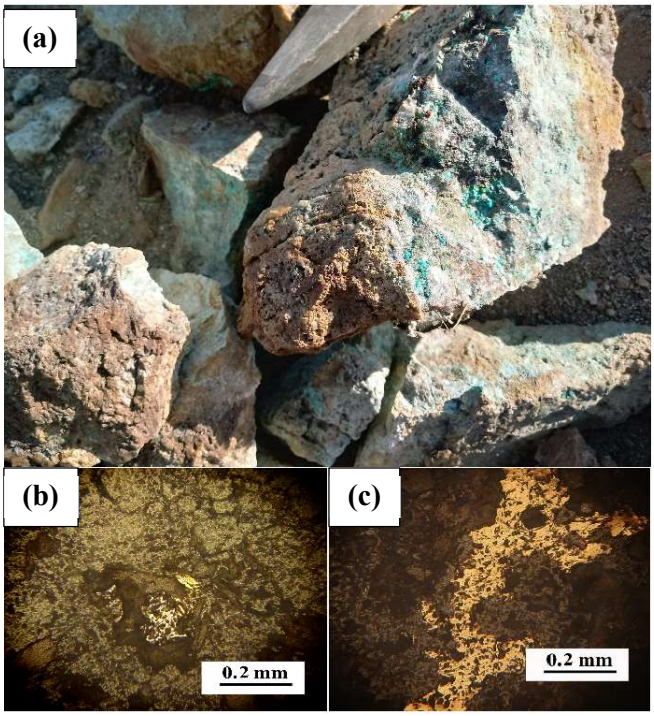


**Figure 3.** a) Outcrop of light gray diorite-quartz diorite. b) Diffuse, faceted magnetite and chalcopyrite crystals within a silicate matrix. c) Chalcopyrite vein associated with secondary quartz and biotite

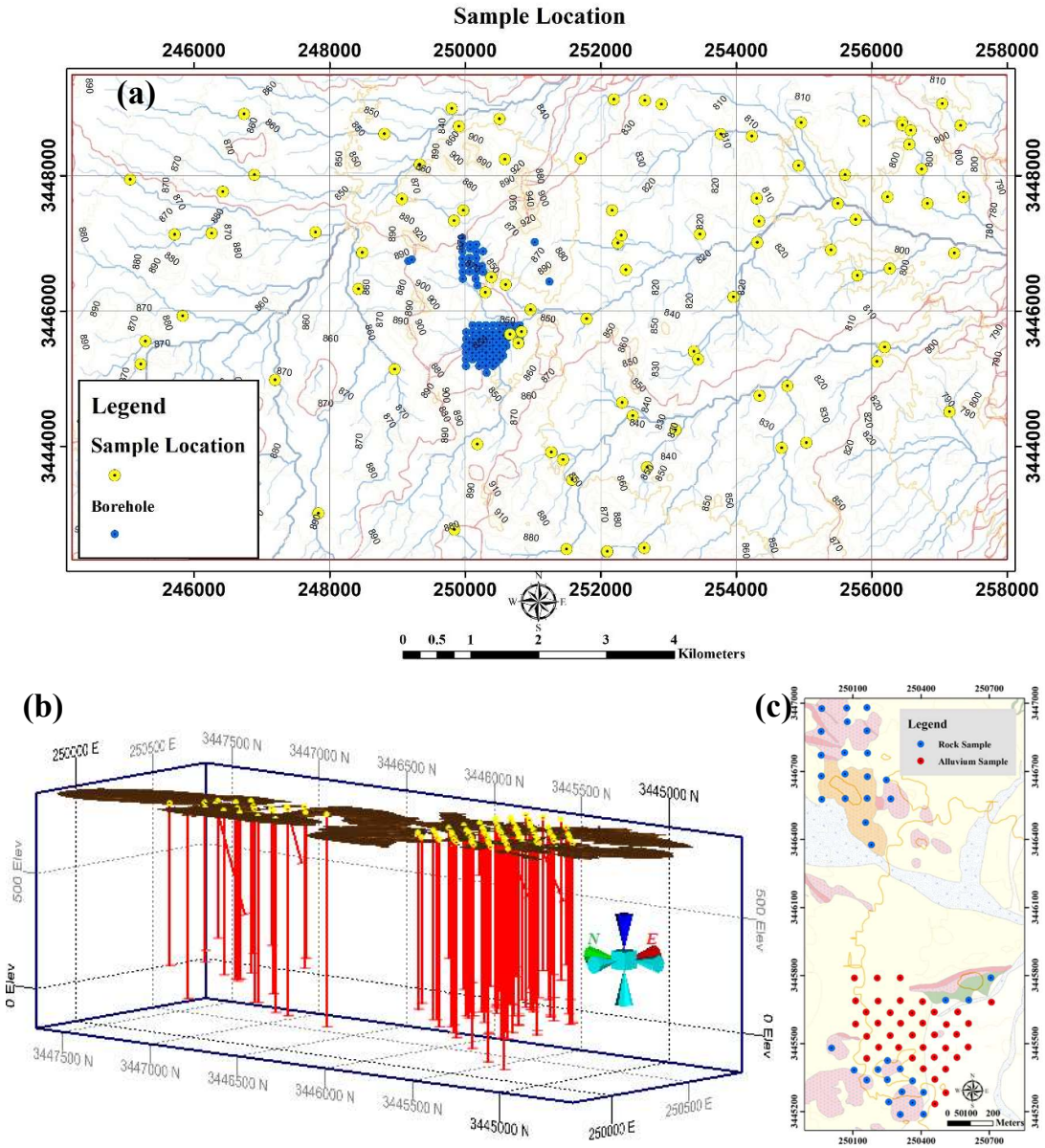


**Figure 4.** a) Location of stream sediment samples b) 3D Model of overburden covering of the Janja deposit c) Location of drilling holes

Correlation analysis and Principal Component Analysis (PCA) were applied to explore elemental associations and corroborate the findings. Elemental distribution maps and three-dimensional overburden models were constructed using Inverse Distance Weighting (IDW) Kriging within ArcGIS Pro. Statistical computations were performed using SPSS (version 26), R (with packages compositions and factoextra), and Python (utilizing the pandas library).

## Results and Discussion

### Centered Log-Ratio (CLR) Transformation

Within the domain of geochemical data analysis, addressing the closure effect embedded in compositional datasets holds utmost importance (Filzmoser et al., 2009; Zuo et al., 2013).

Geochemical compositions, routinely quantified in units such as weight percent (wt%), parts per million (ppm), or parts per billion (ppb), are subject to two critical constraints: their values remain non-negative and sum to a constant value (e.g., 100% or 1,000,000 ppm), while a modification in one component inevitably alters the proportional representation of the others. This condition, known as the closure effect, generates biases in statistical assessments and promotes erroneous correlations stemming from the constant-sum restriction (Chayes, 1960; Pearce, 1968; Pearson, 1897). Simply isolating subsets of the data does not mitigate this issue. As a result, extensive research has emphasized the necessity of transforming geochemical datasets before analysis to ensure compatibility with Euclidean-based multivariate statistical methods (Aitchison, 1982; Buccianti & Grunsky, 2014; Geboy et al., 2013; Pawlowsky-Glahn & Buccianti, 2011; Thiombane et al., 2018).

Log-ratio transformation strategies for analyzing compositional data are classified into three primary categories:

- Additive Log-Ratio (ALR)
- Centered Log-Ratio (CLR)
- Isometric Log-Ratio (ILR)

(Khammar et al., 2021). These techniques are formulated to eliminate the structural dependency arising from the constant-sum property typical of compositional data.

Among these approaches, the Centered Log-Ratio (CLR) transformation stands out as a favored technique due to its simplicity in execution and effectiveness in reducing closure-induced distortions (Ayati et al., 2013). The CLR method entails calculating the natural logarithm of each variable and adjusting it by the geometric mean of all variables (Equation 1), thus enabling a more reliable interpretation of geochemical signatures.

Equation 1:
$$(xi) = \left[ \ln \frac{x_i}{\sqrt[D]{\prod_{i=1}^{D} x_i}}, \dots, \ln \frac{x_D}{\sqrt[D]{\prod_{i=1}^{D} x_i}} \right]$$

A significant advantage of the CLR transformation is its ability to preserve all variables within the analytical process, distinguishing it from the Additive Log-Ratio (ALR) method, which mandates the selection and omission of a reference variable. In comparison, the Isometric Log-Ratio (ILR) technique reconfigures the dataset into an orthogonal coordinate system, diminishing dimensionality while delivering elevated accuracy for intricate analyses; however, its interpretative challenges arise from computational complexities (Filzmoser et al., 2008; Graffelman et al., 2018; Hassanpour & Afzal, 2013; Shahbazi et al., 2021).

A pivotal attribute of CLR lies in its capacity to facilitate a thorough examination of geochemical datasets without the exclusion of any components. Nonetheless, this approach is accompanied by certain constraints, notably its lack of compatibility with select multivariate statistical methods, as data transformed by CLR may not fulfill the foundational assumptions of certain statistical frameworks (Aitchison, 1982). Such incompatibilities may present difficulties in applications demanding sophisticated analytical techniques.

To more effectively highlight the distinctions and properties of these approaches, the subsequent table offers a detailed comparison of ALR, CLR, and ILR (Table 1):

The table below presents an in-depth comparative analysis of the Additive Log-Ratio (ALR), Centered Log-Ratio (CLR), and Isometric Log-Ratio (ILR) transformation techniques. This assessment highlights that CLR, due to its optimal balance between precision and ease of application, is often preferred for a broad spectrum of geochemical applications. However, the selection of the most appropriate method depends on the dataset's characteristics, the specific analytical objectives, and the statistical methodologies utilized (Aitchison, 1982). For example, ALR is sufficient for initial exploratory analyses, whereas ILR is more appropriate for advanced

studies requiring detailed modeling (Hassanpour & Afzal, 2013; Shahbazi et al., 2021). Following the identification and correction of outliers, a logarithmic transformation was applied to datasets displaying a log-normal distribution. To assess the normality of the data distribution, the F-function was utilized, calculated from skewness (Sk) and kurtosis (K) parameters (Equation 2).

Equation 2: $$F = 2|Sk| + |3 - K|$$

The closer the F value is to zero, the closer the data distribution is to a normal distribution (Table 2, Figure 5).

**Staged Factor Analysis (SFA)**

Staged Factor Analysis (SFA) represents an advanced multivariate statistical technique that enhances conventional Factor Analysis (FA) by systematically processing geochemical datasets to accurately isolate factors linked to mineralization.

**Table 1.** The table provides a comparison of the Additive Log-Ratio (ALR), Centered Log-Ratio (CLR), and Isometric Log-Ratio (ILR)

| Method | Definition | Advantages | Disadvantages | Applications | Related Methods |
|---|---|---|---|---|---|
| **CLR** | Calculation of the logarithm of each variable divided by the geometric mean of all variables | Preserves all variables, reduces closure effects, easy to implement | Incompatibility with some multivariate statistical methods | Geochemical data analysis, principal component analysis (PCA), clustering | PCA, K-means clustering |
| **ALR** | Calculation of the logarithm of the ratio of each variable to a selected reference variable | Simplicity in calculations, suitable for preliminary analyses | Dependence on the choice of reference variable, exclusion of one variable from analysis | Preliminary geochemical investigations, simple analyses | Univariate analyses, traditional statistical methods |
| **ILR** | Transformation of variables into orthogonal coordinates in the closed data space | High accuracy in advanced analyses, complete removal of structural collinearity | Computational complexity, difficulty in interpreting results | Complex geochemical analyses, advanced modeling | Orthogonal space-based analyses, advanced clustering methods |

**Table 2.** Statistical description of stream sediment samples

| Element | | Cu | Mo | As | Pb | Zn | S | Ag | Sb |
|---|---|---|---|---|---|---|---|---|---|
| **Mean** | | 26.65 | 0.95 | 12 | 24.88 | 72.63 | 404.03 | 0.25 | 1.68 |
| **Median** | | 26 | 0.93 | 10.3 | 19 | 68 | 140 | 0.27 | 1.08 |
| **Std** | | 6.9 | 0.27 | 8.71 | 43.9 | 39.84 | 1071.43 | 0.07 | 4 |
| **Max** | | 103 | 1.83 | 100 | 544 | 538 | 7821 | 0.42 | 44.5 |
| **Skewness** | Raw | 8.92 | 0.47 | 7.66 | 11.01 | 10.53 | 5.19 | -0.27 | 8.81 |
| | LN | 4.04 | -0.03 | 3.58 | 3.24 | 4.23 | 1.86 | -0.7 | 4.45 |
| | CLR | -1.16 | -0.99 | 0.45 | 0.39 | -1.22 | 2.35 | -1.15 | 4.64 |
| **Kurtosis** | Raw | 99.39 | 2.68 | 72.18 | 129.74 | 123.37 | 31.01 | 2.15 | 89.49 |
| | LN | 36.34 | 2.06 | 20.52 | 22.38 | 36.7 | 6.92 | 2.35 | 24.88 |
| | CLR | 5.08 | 10.12 | 4.26 | 6.79 | 4.33 | 8.93 | 6.67 | 30.31 |
| **F** | Raw | 114.24 | 1.26 | 84.5 | 148.76 | 141.42 | 38.39 | 1.39 | 104.11 |
| | LN | 41.41 | 0.99 | 24.67 | 25.87 | 42.16 | 7.64 | 2.05 | 30.79 |
| | CLR | 4.4 | 9.1 | 2.16 | 4.57 | 3.77 | 10.63 | 5.98 | 36.59 |

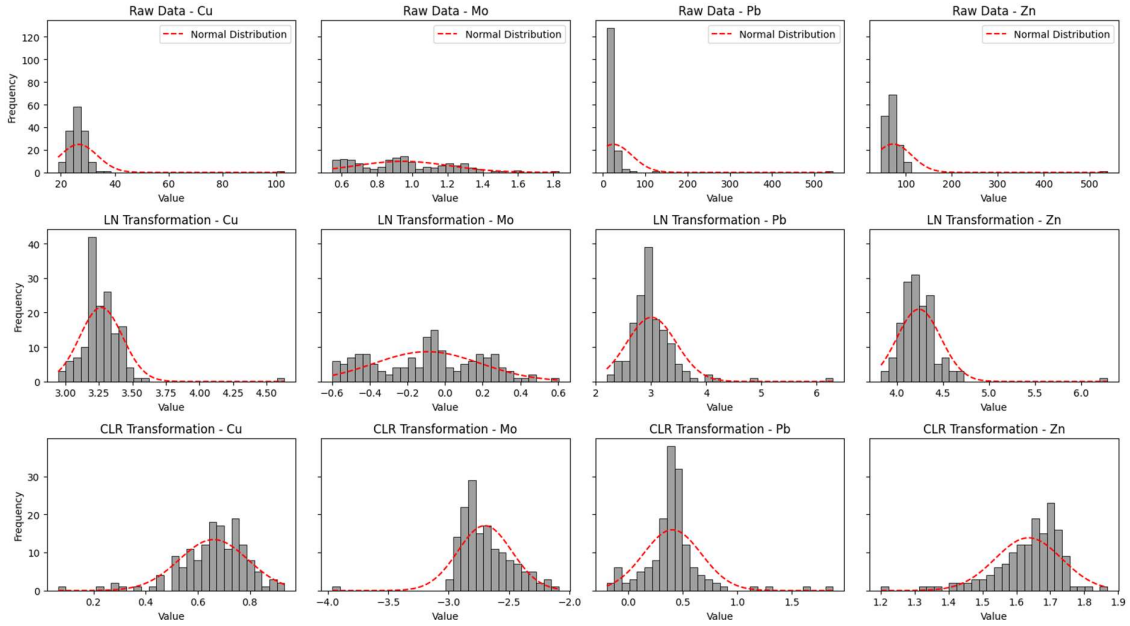


**Figure 5.** Histogram of elements before and after normalization using LN and CLR

This methodology proceeds through a structured, iterative framework involving two key phases: (1) the exclusion of non-informative elements (noise) characterized by low factor loadings (e.g., below a 0.5 threshold), which contribute minimally to any factor, accomplished by iteratively applying factor analysis with varimax rotation until all retained elements display significant loadings; and (2) the identification of factors most strongly correlated with the targeted mineral deposit type, thereby yielding meaningful geochemical signatures. This strategy effectively reduces geochemical noise and improves the detection of multi-element anomalies associated with mineralization, particularly when analyzing stream sediment data (Afzal et al., 2017; Afzal et al., 2016; Farahmandfar et al., 2020; Fyzollahhi et al., 2018; Ghasemzadeh et al., 2019; Imamalipour et al., 2024; Sadeghi et al., 2021; Yousefi et al., 2012, 2014).

SFA provides notable advancements over Stepwise Factor Analysis (SWFA) by not only eliminating noisy elements but also tailoring the analysis to specific mineralization types, thus optimizing factors for geochemical interpretation. To mitigate the closure effect inherent in compositional geochemical data, SFA is commonly paired with preprocessing methods such as logarithmic transformation, ensuring the statistical robustness of the outcomes (Filzmoser et al., 2009). The iterative refinement process and emphasis on mineralization-related factors render SFA more effective than traditional FA, delivering precise and dependable multi-element signatures for delineating geochemical halos surrounding mineral deposits, as evidenced by various exploration studies (Figure 6) (Afzal et al., 2016; Saadati et al., 2020; Yousefi et al., 2012, 2014).

## Geochemical Mineralization Probability Index (GMPI)

The Geochemical Mineralization Probability Index (GMPI) constitutes an advanced fuzzy weighting technique, specifically engineered to improve geochemical mapping during mineral exploration, with a particular focus on stream sediment samples. Initially proposed by Yousefi et al. (2012), this approach converts multi-element factor scores (FSs), commonly obtained from Principal Component Analysis (PCA), into a continuous fuzzy scale ranging from 0 to 1, utilizing the logistic sigmoid function (Equation 3):

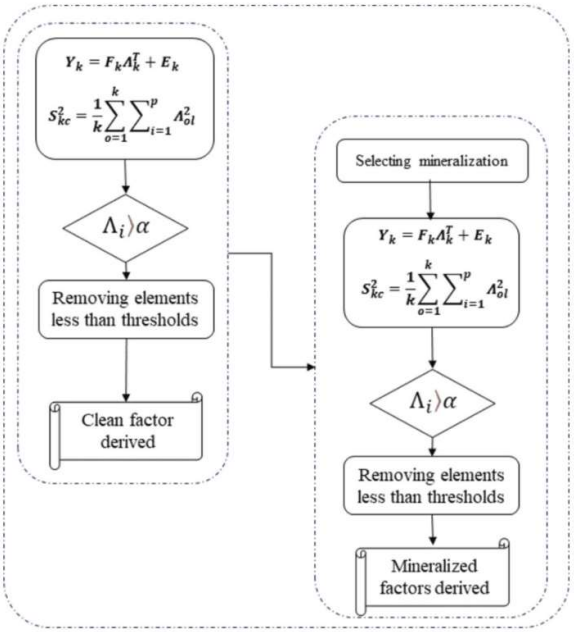


**Figure 6.** The general SFA method of obtaining geochemical signatures of relevance to the target(Hoseinzade & Mokhtari, 2017; Saremi, Maghsoudi, et al., 2024; Yousefi et al., 2014)

Equation 3: $$\mathrm{GMPI} = \frac{1}{1 + e^{-\mathrm{FS}}}$$

In this equation, FS denotes the multi-element signature characterizing a given sample, while e e e represents the base of the natural logarithm (Yousefi & Carranza, 2015; Yousefi et al., 2014). This transformation normalizes exploration data across varying scales, facilitating the synthesis of geochemical and geophysical datasets within Mineral Potential Mapping (MPM). By allocating fuzzy weights to individual samples, GMPI accentuates their relative importance in targeting specific deposit types, thereby enhancing the detection of geochemical anomalies. (Afzal et al., 2016; Imamalipour et al., 2024).

GMPI tackles the challenge of handling continuous and unbounded exploration data within Geographic Information Systems (GIS) by mapping all evidence layers onto the [0, 1] interval, which supports effective data comparison and integration (Yousefi & Carranza, 2017). In application, GMPI applies logistic transformation to fuzzy geochemical and geophysical data—such as magnetic anomalies or signatures derived from Principal Component Analysis (PCA)—and determines parameters like slope (s) and inflection point (i) based on evidence layer values (Yousefi & Carranza, 2015). This technique not only diminishes data dimensionality but also intensifies anomaly prominence, positioning GMPI as a critical instrument for regional mineral exploration. The robust mathematical framework and flexibility of GMPI in accommodating multivariate datasets highlight its significance in contemporary exploration methodologies.

**Semi-Transported Sediments**

Within the semi-transported sediments comprising the overburden of the deposits, notably in regions where alluvial cover thickness surpasses 10 meters (reaching a maximum of 17.2 meters), notable enrichment is detected in Ag (up to 0.6 ppm), Mo (up to 9 ppm), Cd (up to 0.6 ppm), and S (up to 0.5%). It seems that enrichment reflects the pronounced mobility of these elements under oxidative and low pH conditions. The mobility of metals is generally higher in acidic environments and lower in alkaline environments due to pH's impact on metal speciation and solubility. Such a trend is consistent with chemical weathering mechanisms, including sulfide oxidation, alongside chemical and mechanical dispersion within alluvial layers.

Comparable observations have been documented by Anand et al. (2016) in Australian porphyry deposits, linking the enrichment of molybdenum and arsenic to their elevated solubility in alkaline settings (Anand et al., 2016).

Conversely, anomalies of Cu (up to 1490 ppm) and Au (up to 0.15 ppm) are predominantly detected in proximity to outcrops of porphyritic diorite. The mean concentrations of these elements within the overburden zone are recorded at 1212 ppm for copper and 0.1 ppm for gold, suggesting their restricted mobility in this environment. This pattern corroborates findings by Kelley et al. (2004) in Arizona's porphyry belts, which recognize copper and gold as direct indicators of mineralization in areas adjacent to their source (Kelley et al., 2004).

Statistical analysis highlights a marked disparity in element mobility between the overburden and hypogene zones. This distinction emphasizes the pivotal influence of surficial processes, such as erosion and weathering, on the geochemical distribution of elements. Accordingly, this study underscores the necessity of examining geochemical and surficial processes to elucidate mineralization patterns and facilitate the exploration of mineral resources (Table 3). It is worth noting that the average values of elements in the outcrop column refer to the average concentrations of these elements in samples taken from rock outcrops, while the average values of element concentrations in the overburden column refer to the values of concentrations in the cover thickness obtained from drill cores. The thickness of the overburden varies from 10 to 17.2 meters.

By comparing the coefficient of variation (CV) in core samples from the hypogene zone with those from the overburden overlying the mineral deposit, it becomes apparent that the CV for nearly all elements is upper in samples from the hypogene zone compared to those from the overburden (Figure 7). The F-function values for the elements Cu and Au in mineralized diorite outcrops are approximately double those observed in the overburden. Conversely, for elements including Ag, As, Cd, Mo, Pb, S, Sb, and Zn, the F-function values in the overburden is more than those in samples from mineralized diorite outcrops (Figure 8).

**Table 3.** Descriptive statistics of geochemical elements in the Janja area

| | Mean | | | Earth Crust | F | | | CV% | | |
|---|---|---|---|---|---|---|---|---|---|---|
| | Hypogene zone | Outcrops | Overburden | | Hypogene zone | Outcrops | Overburden | Hypogene zone | Outcrops | Overburden |
| **Ag** | 0.97 | 0.28 | 0.6 | 0.08 | 12.2 | 3.5 | 7.5 | 284.54 | 58.47 | 55.09 |
| **Al** | 63215 | 48045 | 61040 | 81300 | 0.8 | 0.6 | 0.8 | 39 | 65 | 25 |
| **As** | 8 | 7 | 11 | 2 | 4.4 | 4 | 6.2 | 141 | 75 | 87 |
| **Au** | 0.32 | 0.15 | 0.1 | 0 | 80.9 | 38.4 | 26.1 | 100.91 | 61.16 | 75.77 |
| **Ca** | 29720 | 13425 | 31275 | 36300 | 0.8 | 0.4 | 0.9 | 52 | 78 | 99 |
| **Cd** | 0.6 | 0.51 | 0.6 | 0 | 3 | 2.5 | 3 | 221.25 | 134.62 | 71.16 |
| **Cu** | 2561 | 1490 | 1212 | 55 | 46.6 | 27.1 | 22 | 68 | 48 | 55 |
| **Fe** | 22881 | 18597 | 26982 | 50000 | 0.5 | 0.4 | 0.5 | 61 | 67 | 33 |
| **K** | 16305 | 11965 | 14290 | 25900 | 0.6 | 0.5 | 0.6 | 45 | 70 | 32 |
| **Mg** | 11346 | 8716 | 11963 | 20900 | 0.5 | 0.4 | 0.6 | 51 | 64 | 37 |
| **Mn** | 235 | 245 | 255 | 950 | 0.2 | 0.3 | 0.3 | 86 | 46 | 45 |
| **Mo** | 54 | 4 | 9 | 2 | 35.9 | 2.5 | 6.2 | 270 | 92 | 134 |
| **Na** | 20397 | 13571 | 12263 | 28300 | 0.7 | 0.5 | 0.4 | 46 | 75 | 43 |
| **Pb** | 35 | 21 | 14 | 13 | 2.7 | 1.6 | 1.1 | 735 | 109 | 82 |
| **S** | 14540 | 364 | 553 | 260 | 55.9 | 1.4 | 2.1 | 78 | 81 | 63 |
| **Sb** | 4 | 2 | 6 | 0 | 21.4 | 10.5 | 29.3 | 308 | 77 | 104 |
| **Sr** | 607 | 353 | 297 | 375 | 1.6 | 0.9 | 0.8 | 29 | 45 | 57 |
| **Zn** | 52 | 36 | 32 | 70 | 0.7 | 0.5 | 0.5 | 588 | 53 | 62 |
| **Zr** | 7 | 10 | 14 | 165 | 0 | 0.1 | 0.1 | 116 | 93 | 74 |

**F = M(janja)/M(Earth)**

**CV% = (SD(janja)/M(janja))*100**

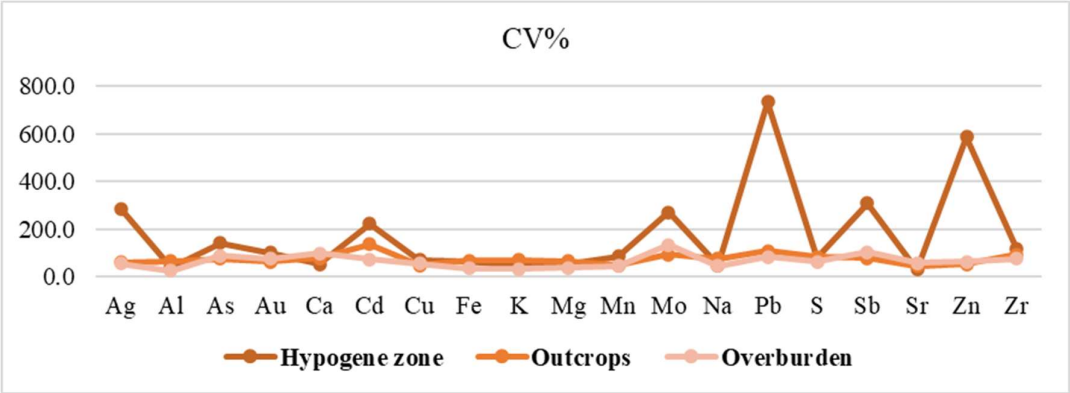


**Figure 7.** The graph shows the values of the coefficients of variations in the concentrations of the investigated elements

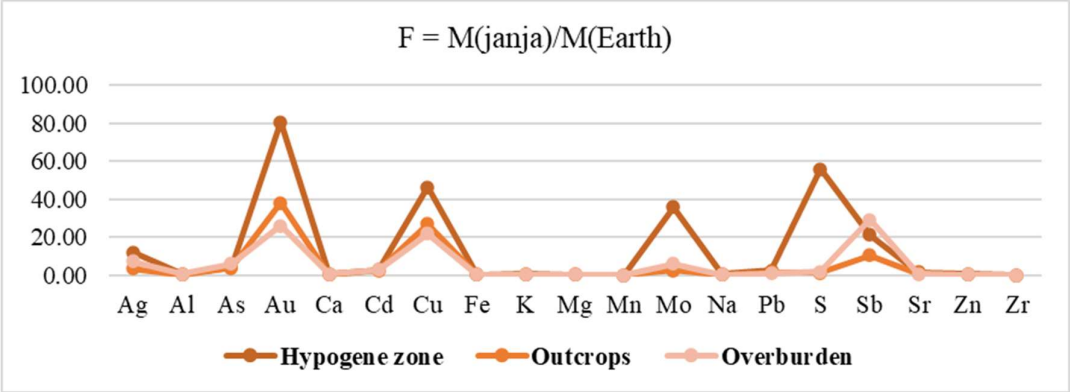


**Figure 8.** F function (enrichment index) values in the hypogene zone, mineralized diorite outcrops and overburden

The findings are consistent with the rotated component matrix derived from the second-stage factor analysis (Table 4), unveiling distinct geochemical signatures within the overburden and hypogene zones. Component F1, exhibiting loadings of 0.95–0.99 for Al, Mg, Na, Fe, K, and Ca, suggests a crustal origin, likely attributable to the natural weathering of regional lithologies. Component F2, with loadings ranging from 0.51 to 0.89 for Sb, As, Cd, Mo, Pb, Ag, and Zn, is indicative of supergene enrichment under oxidative and alkaline environments, corroborating the enhanced mobility of these elements in the overburden, in line with sulfide oxidation and dispersion within alluvial layers. Component F3, displaying loadings of 0.90–0.92 for Cu and Au, signifies primary mineralization proximate to porphyritic diorite outcrops, reflecting their limited mobility in the overburden. These geochemical trends, reinforced by elevated F-function values for Cu and Au in outcrops and for F2 elements in the overburden, highlight the critical influence of surficial processes on element distribution and their pivotal role in mineral exploration strategies.

The GMPI index maps for the elements Au, Cu, Zn, Pb, Ag, Mo, Cd, S, and As in drill core samples are depicted in Figure 8. These maps reveal that anomalies associated with Au, Cu, and Zn are predominantly situated within diorite outcrops across the study area. In contrast, most anomalies are for the other elements. Examples are found in the overburden. The presence of anomalies for elements such as Ag, Mo, Cd, and S. These elements are often considered as mobile elements and are expected to be scarce in surface environments (weathered rocks). The overburden covering the mineral deposit may serve as a pattern for exploring concealed deposits beneath the overburden (Figure 9).

**Table 4.** Rotated component matrix created by SFA (Second stage)

| Rotated Component Matrix[a] | | | |
|---|---|---|---|
| | Component | | |
| **Elements** | **F1** | **F2** | **F3** |
| **Al** | **0.99** | 0.1 | -0.03 |
| **Mg** | **0.98** | 0.08 | -0.04 |
| **Na** | **0.98** | 0.01 | -0.01 |
| **Fe** | **0.98** | 0.13 | -0.02 |
| **K** | **0.97** | 0.14 | 0.04 |
| **Ca** | **0.95** | 0.09 | -0.1 |
| **Sb** | 0.16 | **0.89** | 0.02 |
| **As** | 0.05 | **0.82** | -0.03 |
| **Cd** | 0.3 | **0.8** | 0.17 |
| **Mo** | 0.08 | **0.67** | 0.23 |
| **Pb** | -0.19 | **0.55** | 0.25 |
| **Ag** | 0.43 | **0.54** | 0.08 |
| **Zn** | -0.05 | **0.51** | 0.37 |
| **Cu** | -0.01 | 0.13 | **0.92** |
| **Au** | -0.06 | 0.14 | **0.9** |

The Geochemical Mineralization Probability Index (GMPI) for drill core data, utilizing a threshold of 0.7, evaluates anomalies of the elements Au, Cu, Zn, Pb, Ag, Mo, Cd, S, and As, integrating two principal factors: the first factor encompasses Pb, Ag, Mo, Cd, As, Zn, and Sb, with their anomalies predominantly observed within the overburden; the second factor includes Cu and Au, along with some Zn, with their anomalies primarily detected in porphyritic diorite outcrops. By emphasizing the most pronounced anomalies, this index delineates regions with potential surficial mineralization in porphyritic diorite while concurrently accentuating overburden geochemical signatures for prospecting concealed subsurface deposits. Where both factors display either weak or strong anomalies, their data are harmonized to yield a holistic exploration map (Table 5).

The GMPI index maps for the elements Au, Cu, Zn, Pb, Ag, and Mo in drill core samples are illustrated in Figure 7. These maps demonstrate that anomalies associated with Au, Cu, and Zn are predominantly situated within diorite outcrops across the study area. In contrast, the majority of anomalies for the remaining elements, Pb, Ag, and Mo, are concentrated within the overburden. The occurrence of anomalies for elements such as Ag, Mo, Cd, and S in the overburden overlying the mineral deposit may establish a diagnostic pattern for prospecting concealed deposits beneath this cover (Figure 10).

## Transported Stream Sediments

Geochemical data obtained from stream sediments are classified as compositional data, inherently forming a closed numerical system wherein individual variables exhibit interdependence (Carranza, 2011; Filzmoser et al., 2009). Consequently, factor analysis necessitates prior normalization of these datasets. In this investigation, the Centered Log-Ratio (CLR) transformation is utilized to adjust the multivariate geochemical values, preparing them for conventional factor analysis. Following this, Staged Factor Analysis (SFA) is implemented to derive principal components, uncover latent structures within the multivariate dataset, and diminish the number of variables.

Staged Factor Analysis (SFA) of stream sediment geochemical data effectively elucidates mineralization trends and inter-element associations. The rotated matrix from this analysis delineates three primary factors, characterized by high Kaiser-Meyer-Olkin (KMO) values ranging from 0.753 to 0.851 and a cumulative variance of 84.97%, signifying the robustness of the analytical approach.

**Table 5.** GMPI (mineralization) conditional equation for stepwise factor analysis of exploration borehole data

| | | |
|---|---|---|
| $GMPI_{(F2-2)}$ | $GMPI_{(Pb-Ag-Mo-Cd-As-Zn-Sb)} = \frac{e^{FS_{(Pb-Ag-Mo-Cd-As-Zn-Sb)}}}{1+e^{FS_{(Pb-Ag-Mo-Cd-As-Zn-Sb)}}}$ | |
| $GMPI_{(F3-2)}$ | $GMPI_{(Cu-Au)} = \frac{e^{FS_{(Cu-Au)}}}{1+e^{FS_{(Cu-Au)}}}$ | |
| $GMPI(mineralization)$ | $GMPI(Pb-Ag-Mo-Cd-As-Zn-Sb)$ | $if\ GMPI(Pb-Ag-Mo-Cd-As-Zn-Sb) \geq 0.7\ and\ GMPI(Cu-Au) < 0.7$ |
| | $GMPI(Cu-Au)$ | $if\ GMPI(Cu-Au) \geq 0.7\ and\ GMPI(Pb-Ag-Mo-Cd-As-Zn-Sb) < 0.7$ |
| | $Average(GMPI(Pb-Ag-Mo-Cd-As-Zn-Sb), GMPI(Cu-Au))$ | $if\ GMPI(Pb-Ag-Mo-Cd-As-Zn-Sb) \geq 0.7\ and\ GMPI(Cu-Au) \geq 0.7$ |
| | $Average(GMPI(Pb-Ag-Mo-Cd-As-Zn-Sb), GMPI(Cu-Au))$ | $if\ GMPI(Pb-Ag-Mo-Cd-As-Zn-Sb) < 0.7\ and\ GMPI(Cu-Au) < 0.7$ |

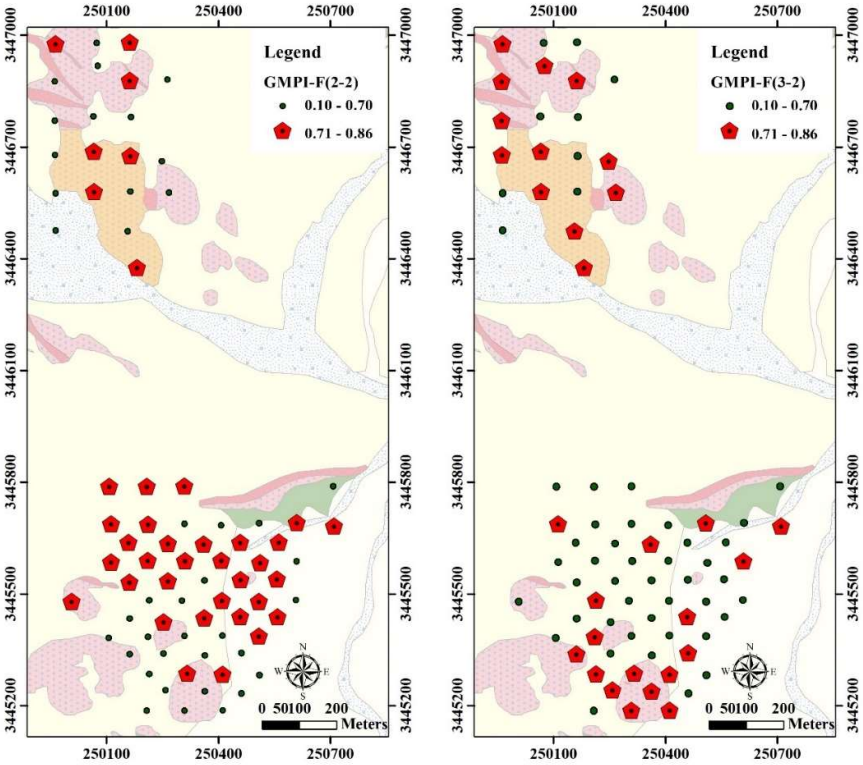


**Figure 9.** Anomaly map of factors obtained from the SFA method using the GMPI method for exploration borehole data; a)F2-2 b) F3-2

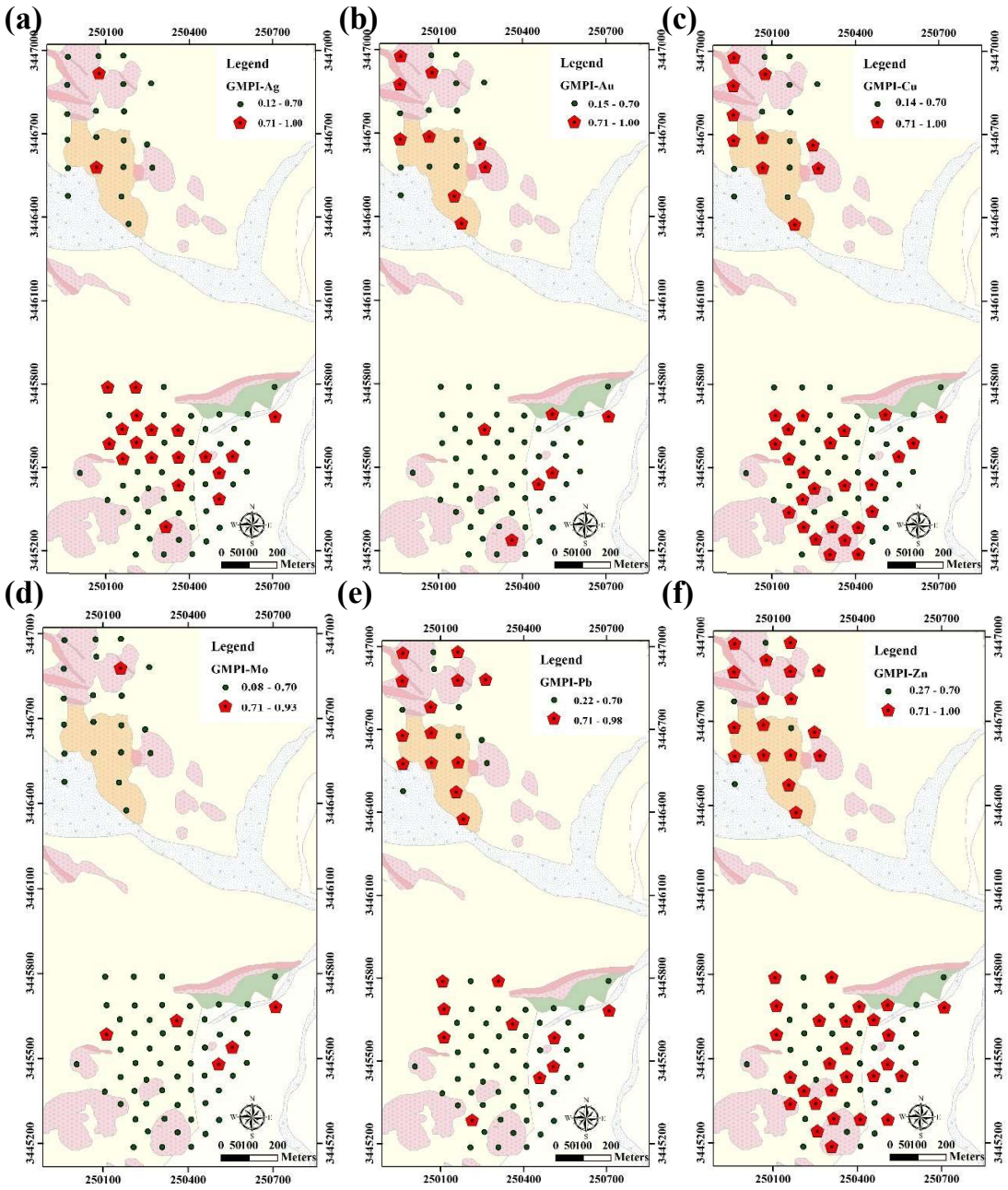


**Figure 10.** Elements anomaly map using the GMPI method for exploration borehole data; a)Ag b)Au c) Cu d)Mo e)Pb f)Zn

In the initial stage, Factor 1 (F1, 47.94%) exhibits a robust correlation with the elements Al, As, Ce, Cr, Mo, Sc, Th, and Yb (loadings > 0.8), indicative of lithogenic phases and the presence of highly mobile elements (As and Mo). Factor 2 (F2, 15.79%) encompasses the elements Fe, V, Co, Mn, La, and Zn, suggesting their adsorption onto iron and manganese oxides. Factor 3 (F3, 8.79%) is defined by elevated loadings for Cd (0.92), Pb (0.83), Ag (0.74), Zn (0.75), and Cu (0.73), signifying porphyry and vein-type sulfide mineralization.

Comparable patterns emerge in the second and third stages. Factor 3 in the second stage and Factor 2 in the third stage reaffirm the chalcophile elements (Cd, Pb, Ag, Zn, Cu). Furthermore, Factor 3 in the third stage is marked by high loadings for Mo (0.89), As (0.87), and S (0.72), highlighting these as highly mobile elements (Table 6).

**Table 6.** The values of factor score in the SFA method for the first, second, and Third steps

| Rotated Component Matrix[a] | | | | | | | | | | | |
|---|---|---|---|---|---|---|---|---|---|---|---|
| | First stage | | | | | Second stage | | | Third stage | | |
| | F1 | F2 | F3 | F4 | F5 | F1 | F2 | F3 | F1 | F2 | F3 |
| **Ag** | 0.09 | 0.14 | **0.74** | 0.30 | 0.27 | 0.11 | 0.13 | **0.77** | 0.15 | **0.77** | 0.12 |
| **Au** | 0.12 | 0.23 | -0.04 | -0.02 | -0.26 | - | - | - | - | - | - |
| **Al** | **0.92** | 0.02 | 0.08 | 0.20 | -0.07 | **0.94** | -0.08 | 0.08 | - | - | - |
| **As** | **0.89** | 0.15 | 0.15 | 0.00 | -0.07 | **0.89** | 0.08 | 0.14 | 0.26 | 0.12 | **0.87** |
| **Ca** | -0.87 | -0.01 | -0.03 | 0.37 | -0.08 | - | - | - | - | - | - |
| **Cd** | -0.04 | -0.09 | **0.92** | -0.13 | -0.07 | -0.05 | -0.10 | **0.91** | -0.08 | **0.92** | -0.03 |
| **Ce** | **0.86** | 0.42 | 0.09 | 0.13 | 0.10 | **0.91** | 0.34 | 0.10 | - | - | - |
| **Co** | 0.32 | **0.85** | 0.26 | -0.13 | 0.20 | 0.38 | **0.85** | 0.27 | **0.91** | 0.25 | 0.21 |
| **Cr** | **0.82** | 0.47 | 0.16 | -0.15 | 0.11 | **0.83** | 0.44 | 0.15 | - | - | - |
| **Cu** | 0.33 | 0.39 | **0.73** | 0.15 | -0.13 | 0.40 | 0.30 | **0.72** | 0.41 | **0.70** | 0.33 |
| **Fe** | 0.25 | **0.89** | 0.26 | -0.17 | 0.00 | 0.30 | **0.89** | 0.26 | **0.94** | 0.22 | 0.15 |
| **La** | 0.42 | **0.76** | 0.09 | 0.25 | 0.25 | **0.51** | **0.70** | 0.12 | - | - | - |
| **Li** | -0.11 | -0.10 | -0.01 | **0.96** | 0.05 | - | - | - | - | - | - |
| **Mg** | -0.84 | -0.06 | -0.05 | 0.25 | 0.42 | - | - | - | - | - | - |
| **Mn** | **0.65** | **0.70** | 0.26 | 0.01 | 0.03 | **0.70** | **0.65** | 0.26 | **0.77** | 0.23 | **0.57** |
| **Mo** | **0.85** | 0.23 | 0.11 | 0.26 | 0.04 | **0.88** | 0.15 | 0.11 | 0.31 | 0.09 | **0.89** |
| **Ni** | -0.05 | 0.37 | 0.09 | -0.01 | **0.83** | - | - | - | - | - | - |
| **P** | -0.88 | 0.07 | -0.04 | 0.26 | -0.07 | - | - | - | - | - | - |
| **Pb** | 0.19 | 0.25 | **0.83** | -0.15 | 0.18 | 0.19 | 0.27 | **0.84** | 0.32 | **0.84** | 0.15 |
| **S** | **0.54** | -0.41 | 0.18 | 0.26 | -0.04 | **0.56** | -0.50 | 0.18 | -0.39 | 0.16 | **0.72** |
| **Sb** | 0.40 | 0.17 | 0.34 | 0.14 | 0.36 | - | - | - | - | - | - |
| **Sc** | **0.84** | 0.43 | 0.18 | -0.12 | -0.05 | **0.87** | 0.36 | 0.17 | - | - | - |
| **Th** | **0.69** | 0.33 | 0.23 | 0.21 | -0.02 | **0.74** | 0.24 | 0.24 | - | - | - |
| **V** | -0.05 | **0.93** | 0.17 | 0.02 | 0.04 | 0.02 | **0.94** | 0.17 | **0.94** | 0.13 | -0.10 |
| **Yb** | **0.90** | 0.35 | 0.13 | -0.13 | -0.10 | **0.91** | 0.29 | 0.12 | - | - | - |
| **Zn** | 0.24 | **0.57** | **0.75** | -0.03 | 0.01 | 0.29 | **0.55** | **0.75** | **0.61** | **0.73** | 0.20 |
| **KMO and Bartlett's Test** | | | 0.851 | | | | 0.833 | | | 0.753 | |
| **Variance (%)** | 47.94 | 15.79 | 8.79 | 6.78 | 4.07 | 56.59 | 16.37 | 11.43 | 52.54 | 16.72 | 15.70 |
| **Cumulative variance** | 47.94 | 63.73 | 72.52 | 79.30 | 83.37 | 56.59 | 72.96 | 84.39 | 52.54 | 69.27 | 84.97 |

These observations align with the arid environmental conditions prevalent in the region, where restricted chemical weathering promotes the mechanical dispersion of low-mobility elements, while oxidative processes enhance the transport of soluble species. (Mauad et al., 2015; Mora et al., 2018; Tazikeh et al., 2018). Factor analysis delineates two distinct element assemblages: (1) the Cu, Pb, Zn, Ag, and Cd group, characterized by anomalies proximate to their source, ideal for direct detection of mineralization; and (2) the Mo, As, and S group, exhibiting wide dispersion halos, essential for tracing concealed deposits beneath alluvial cover.

Consequently, strategic stream sediment sampling, prioritizing Cu, Pb, and Zn to pinpoint near-source targets and Mo and As for regional exploration, can enhance exploration efficiency in this structurally intricate region (Figure 11, Table 7).

The geochemical behavior and mobility of key elements, including Cd, Pb, As, Zn, Cu, Mo, Ag, and S, within the stream sediments of the Janja porphyry deposit are influenced by mineralogical composition, arid climatic conditions, and weathering mechanisms. Situated in a desert landscape characterized by gentle topography and extensive Quaternary alluvial cover, the Janja region encompasses a porphyry mineralization system linked to diorite to granodiorite intrusions and polymetallic sulfide veins. Elements such as Cu, Pb, Zn, Ag, and Cd, predominantly hosted in sulfide minerals like chalcopyrite ($CuFeS_2$), galena (PbS), and sphalerite (ZnS), demonstrate low to moderate mobility owing to their adsorption onto secondary phases, including iron oxides/hydroxides (e.g., hematite and goethite) and clay minerals (e.g., illite and kaolinite).

**Table 7.** GMPI (mineralization) conditional equation for stepwise factor analysis of stream sediment data

| | | |
|---|---|---|
| $GMPI_{(F2-3)}$ | $GMPI_{(Pb-Ag-\ Cd-Zn-Cu)} = \frac{e^{FS_{(Pb-Ag-\ Cd-Zn-Cu)}}}{1+e^{FS_{(Pb-Ag-\ Cd-Zn-Cu)}}}$ | |
| $GMPI_{(F3-3)}$ | $GMPI_{(As-Mo-Mn-S)} = \frac{e^{FS_{(As-Mo-Mn-S)}}}{1+e^{FS_{(As-Mo-Mn-S)}}}$ | |
| $GMPI(mineralization)$ | $GMPI(Pb-Ag-\ Cd-Zn-Cu)$ | $if\ GMPI(Pb-Ag-\ Cd-Zn-Cu) \geq 0.7\ and\ GMPI(As-Mo-Mn-S) < 0.7$ |
| | $GMPI(As-Mo-Mn-S)$ | $if\ GMPI(As-Mo-Mn-S) \geq 0.7\ and\ GMPI(Pb-Ag-\ Cd-Zn-Cu) < 0.7$ |
| | $Average(GMPI(Pb-Ag-\ Cd-Zn-Cu), GMPI(As-Mo-Mn-S))$ | $if\ GMPI(Pb-Ag-\ Cd-Zn-Cu) \geq 0.7\ and\ GMPI(As-Mo-Mn-S) \geq 0.7$ |
| | $Average(GMPI(Pb-Ag-\ Cd-Zn-Cu), GMPI(As-Mo-Mn-S))$ | $if\ GMPI(Pb-Ag-\ Cd-Zn-Cu) < 0.7\ and\ GMPI(As-Mo-Mn-S) < 0.7$ |

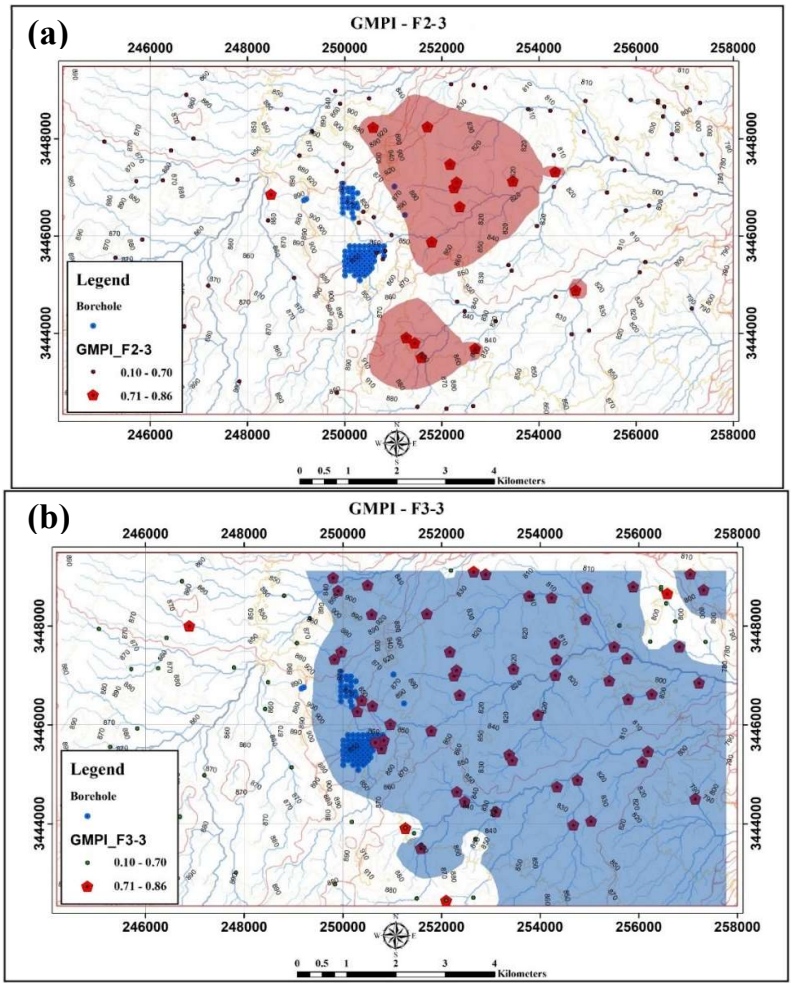


**Figure 11.** Anomaly map of factors obtained from the SFA method using the GMPI method for stream sediment data; a)F2-3, b) F3-3

In the arid, oxidative environment with neutral to alkaline pH driven by carbonate presence, these elements precipitate swiftly near their source, generating concentrated geochemical anomalies in stream sediments adjacent to the porphyry stock and mineralized veins. Their restricted dispersion is largely governed by mechanical erosion and transport through seasonal streams, further limited by minimal moisture and subdued chemical weathering processes (Figure 12).

In contrast, elements such as Mo, As, and S exhibit elevated mobility due to the oxidative weathering of sulfide minerals and their conversion into soluble forms. Molybdenum, present as molybdenite ($MoS_2$), oxidizes to molybdate ($MoO_4^{2-}$), facilitating its transport via surface or groundwater and forming extensive dispersion halos in stream sediments. Arsenic, occurring in arsenopyrite (FeAsS) or as a trace constituent in other sulfides, transforms into arsenate ($AsO_4^{3-}$) and, if not retained by iron oxides, is transported over greater distances, producing significant anomalies in distal sediments. Sulfur, originating from sulfide oxidation to sulfate ($SO_4^{2-}$), disperses rapidly within the stream network. The pronounced mobility of Mo, As, and S positions them as critical geochemical tracers for regional exploration of concealed mineralization in alluvial-covered terrains, whereas low-mobility elements (Cu, Pb, Zn, Ag, and Cd) act as precise indicators of proximal sources. These contrasting mobility profiles, molded by the arid, oxidative conditions and dominant mechanical transport in the Janja region, offer a robust foundation for investigating porphyry systems in desert settings (Figure 12).

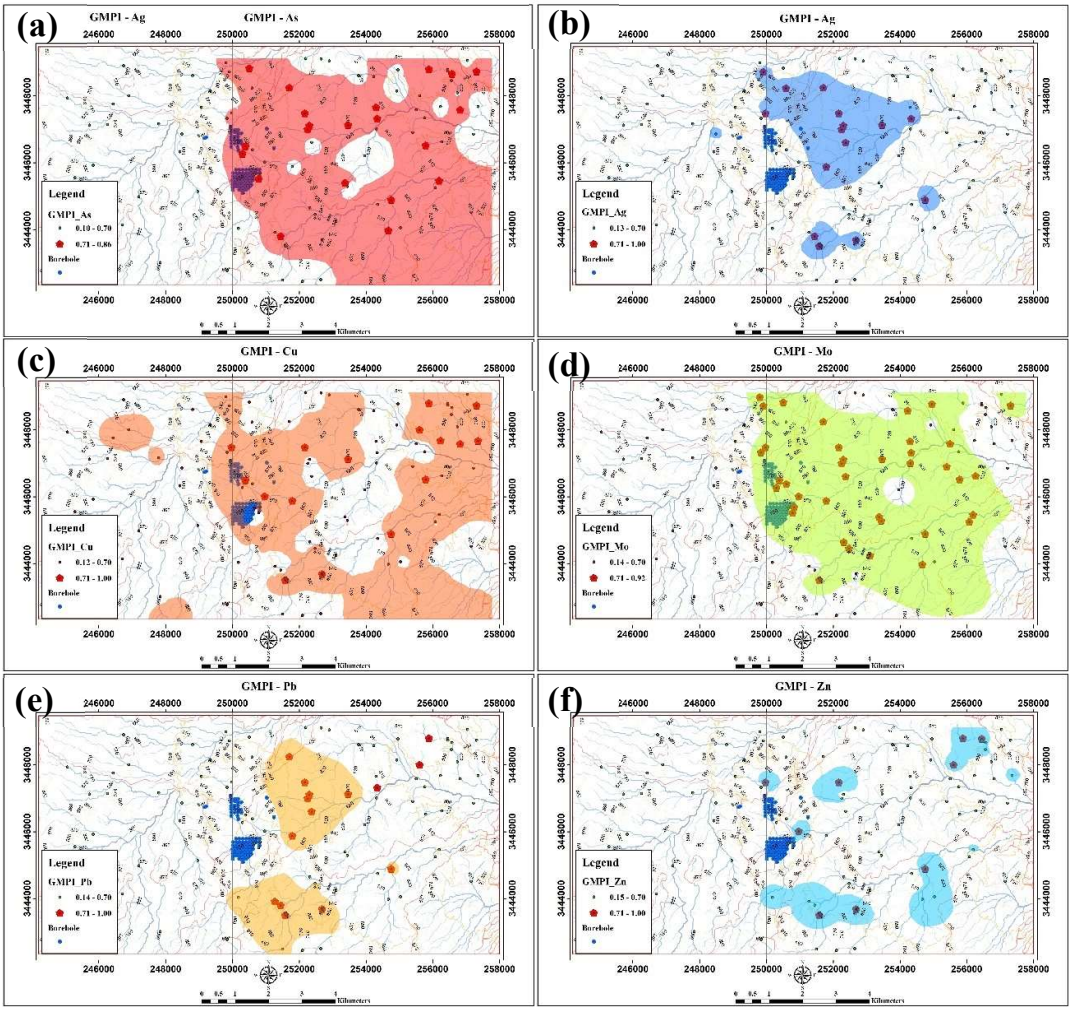


**Figure 12.** Elements anomaly map using the GMPI method for stream sediment data; a)As b)Ag c)Cu d)Mo e)Pb f)Zn

## Conclusion

This investigation establishes a robust and innovative geochemical exploration framework for the Janja porphyry copper deposit, situated within the Zabol–Zahedan–Saravan subzone of eastern Iran, effectively addressing the substantial challenges posed by its extensive alluvial cover. By leveraging advanced multivariate statistical methods ,such as the Centered Log-Ratio (CLR) transformation, Staged Factor Analysis (SFA), and the Geochemical Mineralization Prediction Index (GMPI) ,this study successfully delineates geochemical anomaly patterns linked to concealed porphyry and vein-type mineralization. The analysis of 153 stream sediment samples and 16,300 drill core samples from 74 boreholes yields a comprehensive dataset that elucidates distinct elemental behaviors under arid climatic conditions.

The findings highlight two primary geochemical signatures essential for exploration. Firstly, low-mobility elements, including Cu, Pb, Zn, Ag, and Cd, display concentrated anomalies adjacent to porphyritic diorite outcrops, with average Cu concentrations of 2,561.4 ppm in the hypogene zone and 1,211.53 ppm in the overburden. These elements, predominantly hosted in sulfide minerals such as chalcopyrite, galena, and sphalerite, function as direct indicators of near-source mineralization, exhibiting limited dispersion due to mechanical transport and adsorption onto secondary phases (e.g., iron oxides and clay minerals) within the arid, oxidative setting. Secondly, high-mobility elements, namely Mo, As, and S, develop extensive dispersion halos in stream sediments, with enrichment indices up to five times the Clarke values in the semi-transitional overburden (e.g., Mo up to 9 ppm, S up to 5%). Mobilized through oxidative weathering of sulfides into soluble forms (e.g., molybdate, arsenate, and sulfate), these elements serve as critical pathfinders for detecting concealed deposits beneath alluvial cover.

The CLR transformation effectively addresses the closure effect inherent in compositional geochemical data, enabling robust multivariate analysis. SFA enhances this process by distinguishing three elemental categories in stream sediment data: (1) lithogenic elements (Al, Fe, Mn), (2) sulfide-associated elements (Cu, Pb, Zn, Ag), and (3) mobile elements (Mo, As, S). These categories underscore the interplay among lithological influences, mineralization processes, and surficial dispersion dynamics. The GMPI, employing a threshold of 0.7, synthesizes these multi-element signatures into spatial anomaly maps, emphasizing regions with prominent anomalies in diorite outcrops for Cu and Au, while recognizing overburden anomalies for Ag, Mo, Cd, and S as markers of hidden mineralization.

These results carry significant implications for porphyry copper exploration in covered terrains globally. The recognition of Ag, Mo, Cd, and S as pathfinder elements in semi-transported overburden provides a practical approach for targeting concealed deposits, particularly in arid regions where conventional exploration techniques prove less effective. The proposed framework, integrating CLR, SFA, and GMPI, offers a scalable and versatile methodology that boosts exploration efficiency by refining sampling strategies and reducing drilling costs in geologically complex settings. For example, focused stream sediment sampling targeting Cu, Pb, and Zn can identify near-source targets, whereas sampling for Mo and As can guide regional prospecting efforts.

Moreover, this study emphasizes the vital role of integrating geochemical, geological, and spatial data to model subsurface mineral systems. The observed disparities in element mobility between the hypogene and overburden zones, supported by elevated coefficients of variation and F-function values in the overburden, underscore the impact of surficial processes such as erosion, sedimentation, and chemical weathering on geochemical signatures. These insights enhance the understanding of element dynamics in desert environments, laying the groundwork for future investigations into the geochemical evolution of porphyry systems.

The large amount of data from exploratory drilling can be a criterion for validating the methods used in this research. The geochemical patterns derived from 153 stream sediment

samples were rigorously compared with results from 16,300 drill core samples to validate the mineralization model. Statistical analyses, including correlation coefficients and cross-validation of elemental anomalies, confirmed a high degree of consistency between the datasets, supporting the reliability of the Staged Factor Analysis (SFA) and Geochemical Mineralization Probability Index (GMPI) methods in identifying the Janja Cu-Au porphyry deposit.

In summary, this research not only advances the exploration of the Janja porphyry copper deposit but also establishes a benchmark for geochemical studies in analogous covered terrains worldwide. By delivering a rigorous, data-informed strategy for identifying concealed mineralization, this study addresses the global demand for critical metals like Cu, Au, and Mo, fostering more sustainable and cost-efficient mineral exploration practices. Future research should prioritize the incorporation of geophysical techniques and machine learning approaches to further refine anomaly detection and improve the predictive precision of mineral prospectivity mapping in such challenging environments.

## Acknowlegments

We would like to thank the staff of Iranian Minerals Procurement and Production Company (IMPASCO) for giving permission to have access to the analysis of samples of diamond drill cores essential to furthering the studies of this investigation.

This research was made possible with the aid of the office of the vice-chancellor for ‘Research and Technology’ at Urmia University. We acknowledge their support.

## Conflicts of interest

The authors declare that they have no known competing financial interests or personal relationships that could have appeared to influence the work reported in this paper. This study was supported by the office of the Vice-Chancellor for Research and Technology at Urmia University, and data access was provided by the Iranian Minerals Procurement and Production Company (IMPASCO). No other financial or non-financial interests are associated with this research.

## References

Afzal, P., Ahmadi, K., & Rahbar, K. (2017). Application of fractal-wavelet analysis for separation of geochemical anomalies. Journal of African Earth Sciences, 128, 27-36.

Afzal, P., Tehrani, M. E., Ghaderi, M., & Hosseini, M. R. (2016). Delineation of supergene enrichment, hypogene and oxidation zones utilizing staged factor analysis and fractal modeling in Takht-e-Gonbad porphyry deposit, SE Iran. Journal of Geochemical Exploration, 161, 119-127.

Aitchison, J. (1982). The statistical analysis of compositional data. Journal of the Royal Statistical Society: Series B (Methodological), 44(2), 139-160.

Anand, R., Lintern, M., Noble, R., Aspandiar, M., Macfarlane, C., Hough, R., Stewart, A., Wakelin, S., Townley, B., & Reid, N. (2014). Geochemical dispersion through transported cover in regolith-dominated terrains-toward an understanding of process.

Anand, R. R., Aspandiar, M. F., & Noble, R. R. (2016). A review of metal transfer mechanisms through transported cover with emphasis on the vadose zone within the Australian regolith. Ore Geology Reviews, 73, 394-416.

Ayari, I., Ben Alaya, M., & Zammouri, M. (2022). Hydrogeochemical characterization and suitability of groundwater for drinking and irrigation in Menzel Bourguiba aquifers (Northeastern Tunisia). Environmental Monitoring and Assessment, 194(8), 524.

Ayati, F., Yavuz, F., Asadi, H. H., Richards, J. P., & Jourdan, F. (2013). Petrology and geochemistry of calc-alkaline volcanic and subvolcanic rocks, Dalli porphyry copper–gold deposit, Markazi

Province, Iran. International Geology Review, 55(2), 158-184.
Barak, S., Imamalipour, A., & Abedi, M. (2024). Employing multiple prospectivity mapping and exploration targeting, a case study from the Sonajil porphyry copper deposit, north-western Iran. Bulletin of Geophysics and Oceanography, DOI, 10.
Barak, S., Imamalipour, A., Abedi, M., Bahroudi, A., & Khalifani, F. M. (2021). Comprehensive modeling of mineral potential mapping by integration of multiset geosciences data. Geochemistry, 81(4), 125824.
Batanova, V. G., & Sobolev, A. V. (2000). Compositional heterogeneity in subduction-related mantle peridotites, Troodos massif, Cyprus. Geology, 28(1), 55-58.
Bigdeli, A., Maghsoudi, A., & Ghezelbash, R. (2023). Recognizing geochemical anomalies associated with mineral resources using singularity analysis and random forest models in the Torud-Chahshirin Belt, Northeast Iran. Minerals, 13(11), 1399.
Buccianti, A., & Grunsky, E. (2014). Compositional data analysis in geochemistry: are we sure to see what really occurs during natural processes? In (Vol. 141, pp. 1-5): Elsevier.
Butt, C. R., Lintern, M., & Anand, R. (2000). Evolution of regoliths and landscapes in deeply weathered terrain—implications for geochemical exploration. Ore Geology Reviews, 16(3-4), 167-183.
Camp, V., & Griffis, R. (1982). Character, genesis and tectonic setting of igneous rocks in the Sistan suture zone, eastern Iran. Lithos, 15(3), 221-239.
Carranza, E. J. M. (2008). Geochemical anomaly and mineral prospectivity mapping in GIS. Elsevier.
Carranza, E. J. M. (2011). Analysis and mapping of geochemical anomalies using logratio-transformed stream sediment data with censored values. Journal of Geochemical Exploration, 110(2), 167-185.
Chayes, F. (1960). On correlation between variables of constant sum. Journal of Geophysical research, 65(12), 4185-4193.
Cheng, Q., Agterberg, F. P., & Bonham-Carter, G. F. (1996). A spatial analysis method for geochemical anomaly separation. Journal of Geochemical exploration, 56(3), 183-195.
Cooke, D., Hollings, P., Wilkinson, J., Tosdal, R., & Turekian, H. (2014). 13.14—Geochemistry of porphyry deposits. Treatise on geochemistry, 13, 357-381.
Esmaeiloghli, S., Lima, A., & Sadeghi, B. (2024). Lithium exploration targeting through robust variable selection and deep anomaly detection: an integrated application of sparse principal component analysis and stacked autoencoders. Geochemistry, 84(4), 126111.
Esmaeiloghli, S., Tabatabaei, S. H., Hosseini, S., Deville, Y., & Carranza, E. J. M. (2024). Blind source separation of spectrally filtered geochemical signals to recognize multi-depth ore-related enrichment patterns. Mathematical Geosciences, 56(6), 1255-1283.
Fallara, F., Legault, M., & Rabeau, O. (2006). 3-D integrated geological modeling in the Abitibi Subprovince (Québec, Canada): Techniques and applications. Exploration and Mining Geology, 15(1-2), 27-43.
Farahmandfar, Z., Jafari, M., Afzal, P., & Ashja Ardalan, A. (2020). Description of gold and copper anomalies using fractal and stepwise factor analysis according to stream sediments in NW Iran. Geopersia, 10(1), 135-148.
Filzmoser, P., Hron, K., & Reimann, C. (2009). Principal component analysis for compositional data with outliers. Environmetrics: The Official Journal of the International Environmetrics Society, 20(6), 621-632.
Filzmoser, P., Maronna, R., & Werner, M. (2008). Outlier identification in high dimensions. Computational statistics & data analysis, 52(3), 1694-1711.
Fyzollahhi, N., Torshizian, H., Afzal, P., & Jafari, M. R. (2018). Determination of lithium prospects using fractal modeling and staged factor analysis in Torud region, NE Iran. Journal of Geochemical Exploration, 189, 2-10.
Geboy, N. J., Olea, R. A., Engle, M. A., & Martín-Fernández, J. A. (2013). Using simulated maps to interpret the geochemistry, formation and quality of the Blue Gem coal bed, Kentucky, USA. International Journal of Coal Geology, 112, 26-35.
Ghasemzadeh, S., Maghsoudi, A., Yousefi, M., & Mihalasky, M. J. (2019). Stream sediment geochemical data analysis for district-scale mineral exploration targeting: Measuring the performance of the spatial U-statistic and CA fractal modeling. Ore Geology Reviews, 113, 103115.
Ghasemzadeh, S., Maghsoudi, A., Yousefi, M., & Mihalasky, M. J. (2022). Information value-based geochemical anomaly modeling: A statistical index to generate enhanced geochemical signatures for

mineral exploration targeting. Applied geochemistry, 136, 105177.
Graffelman, J., Pawlowsky-Glahn, V., Egozcue, J. J., & Buccianti, A. (2018). Exploration of geochemical data with compositional canonical biplots. Journal of Geochemical Exploration, 194, 120-133.
Griffis, R. J., Camp, V.E., Bell, I.R., Johns, G.W., Willoughby, N.O.and Tirrul, R. (1990). Geological map of Khonik.
Grunsky, E., & de Caritat, P. (2019). Geochemistry: Exploration, Environment, Analysis.
Grunsky, E. C. (2010). The interpretation of geochemical survey data.
Grunsky, E. C., Drew, L. J., & Sutphin, D. M. (2009). Process recognition in multi-element soil and stream-sediment geochemical data. Applied geochemistry, 24(8), 1602-1616.
Hagemann, S. G., Lisitsin, V., & Huston, D. (2016). Mineral system analysis: Quo vadis. Ore Geology Reviews, 76, 504-522.
Hajihosseinlou, M., Maghsoudi, A., & Ghezelbash, R. (2023). A novel scheme for mapping of MVT-type Pb–Zn prospectivity: LightGBM, a highly efficient gradient boosting decision tree machine learning algorithm. Natural resources research, 32(6), 2417-2438.
Hajihosseinlou, M., Maghsoudi, A., & Ghezelbash, R. (2024a). Geochemical Anomaly Detection and Pattern Recognition: A Combined Study of the Apriori Algorithm, Principal Component Analysis, and Spectral Clustering. Minerals, 14(12), 1202.
Hajihosseinlou, M., Maghsoudi, A., & Ghezelbash, R. (2024b). Intelligent mapping of geochemical anomalies: Adaptation of DBSCAN and mean-shift clustering approaches. Journal of Geochemical Exploration, 258, 107393.
Hassanpour, S., & Afzal, P. (2013). Application of concentration–number (C–N) multifractal modeling for geochemical anomaly separation in Haftcheshmeh porphyry system, NW Iran. Arabian Journal of Geosciences, 6, 957-970.
Hong, J., Khalil, Y. S., Narejo, A. A., Yang, X., Khan, T., Wang, Z., Tang, H., Zhang, H., Yang, B., & Li, W. (2025). Magmatic Evolution at the Saindak Cu-Au Deposit: Implications for the Formation of Giant Porphyry Deposits. Minerals, 15(8), 768.
Hoseinzade, Z., & Mokhtari, A. R. (2017). A comparison study on detection of key geochemical variables and factors through three different types of factor analysis. Journal of African Earth Sciences, 134, 557-563.
Hosseini-Dinani, H., & Aftabi, A. (2016). Vertical lithogeochemical halos and zoning vectors at Goushfil Zn–Pb deposit, Irankuh district, southwestern Isfahan, Iran: Implications for concealed ore exploration and genetic models. Ore Geology Reviews, 72, 1004-1021.
Hou, Z.-Q., Gao, Y.-F., Qu, X.-M., Rui, Z.-Y., & Mo, X.-X. (2004). Origin of adakitic intrusives generated during mid-Miocene east–west extension in southern Tibet. Earth and Planetary Science Letters, 220(1-2), 139-155.
Imamalipour, A., Barak, S., & Haghighi, A. (2024). Leveraging EDA, Fractal Analysis, SFA, and GMPI for Identifying Geochemical Anomalies in Siah Cheshmeh Ophiolite Area, NW Iran. Geopersia(Articles in Press).
IMPASCO. (2022). The geological map of the study area at a scale of 1:5000.
Kelley, D., Cameron, E., Southam, G., Muhling, J., Goldfrab, R., Vielreicher, F., Stumpfi, E., Grove, D., & Kenworthy, S. (2004). Secondary geochemical dispersion through transported overburden. SEG, Perth, 4.
Lowell, J. D., & Guilbert, J. M. (1970). Lateral and vertical alteration-mineralization zoning in porphyry ore deposits. Economic geology, 65(4), 373-408.
Macklin, M., Ridgway, J., Passmore, D., & Rumsby, B. (1994). The use of overbank sediment for geochemical mapping and contamination assessment: results from selected English and Welsh floodplains. Applied geochemistry, 9(6), 689-700.
Mastoi, A. S., Yang, X., Deng, J., Kashani, A. G., & Hakro, A. A. (2020). Geochronological and geochemical studies of adakites from Tethyan Belt, Western Pakistan: A clue to geodynamics and Cu-Au mineralization. International Geology Review, 62(10), 1273-1293.
Mauad, C. R., de LR Wagener, A., Massone, C. G., Aniceto, M. d. S., Lazzari, L., Carreira, R. S., & Farias, C. d. O. (2015). Urban rivers as conveyors of hydrocarbons to sediments of estuarine areas: Source characterization, flow rates and mass accumulation. Science of the Total Environment, 506, 656-666.

Mirzabozorg, S. A. A. S., & Abedi, M. (2023). Recognition of mineralization-related anomaly patterns through an autoencoder neural network for mineral exploration targeting. Applied geochemistry, 158, 105807.

Mora, A., Mahlknecht, J., & Torres-Martínez, A. (2018). Evolution and multivariable analysis of trace elements in groundwater of an agricultural area in a semi-arid region of Mexico. Energy Procedia, 153, 196-201.

Moradi, R., Boomeri, M., & Bagheri, S. (2014). Petrography and geochemistry of intrusive rocks in the Shurchah antimony-bearing area Southeast of Zahedan. Petrology (2228-5210), 5(18).

Moradpouri, F., Ahmadi, S., Ghaedrahmati, R., & Barani, K. (2023). Determination of the erosion level of a porphyry copper deposit using soil geochemistry. Journal of the Southern African Institute of Mining and Metallurgy, 123(2), 103-112.

Muhammad, S., Liu, J., Ullah, I., Chen, X., Ji, L., Zahid, M. A., & Kakar, N. (2024). Oligocene–Miocene arc magmatic activities associated with the giant Reko Diq porphyry Cu–Au deposit, western Chagai arc, Balochistan, Pakistan. Geological Journal, 59(4), 1360-1383.

Murad, F., Ghaffar, A., Ullah, I., Mastoi, A. S., & Zaman, M. T. (2021). The Alteration and Mineralization Characteristics of Miocene Porphyry Cu-Au Deposits of Chagai Magmatic Belt, District Chagai, Balochistan, Pakistan: The Alteration and Mineralization Characteristics of Miocene Porphyry Cu-Au Deposits of Chagai Magmatic Belt, District Chagai, Balochistan, Pakistan. International Journal of Economic and Environmental Geology (IJEEG), 12(1), 1-8.

Nicholson, K., Khan, M., & Mahmood, K. (2010). Geochemistry of the Chagai–Raskoh arc, Pakistan: Complex arc dynamics spanning the Cretaceous to the Quaternary. Lithos, 118(3-4), 338-348.

Olang, P. (2016). Final Report of Geochemical Exploration of Stream Sediments and Heavy Minerals in Janja.

Pawlowsky-Glahn, V., & Buccianti, A. (2011). Compositional data analysis. Wiley Online Library.

Pearce, T. (1968). A contribution to the theory of variation diagrams. Contributions to Mineralogy and Petrology, 19(2), 142-157.

Pearson, K. (1897). Mathematical contributions to the theory of evolution.—on a form of spurious correlation which may arise when indices are used in the measurement of organs. Proceedings of the royal society of london, 60(359-367), 489-498.

Perelló, J., Razique, A., & Schloderer, J. (2008). The Chagai porphyry copper belt, Baluchistan province, Pakistan. Economic geology, 103(8), 1583-1612.

Porwal, A., & Carranza, E. J. M. (2015). Introduction to the Special Issue: GIS-based mineral potential modelling and geological data analyses for mineral exploration. In (Vol. 71, pp. 477-483): Elsevier.

Raeisi, D., Hajsadeghi, S., Hosseinzadehsabeti, E., Babazadeh, S., Lentz, D. R., & Santosh, M. (2023). Exploration targeting in the Shadan porphyry gold–copper deposit, Lut block, Iran: Analysis of spatial distribution of sheeted veins and Lithogeochemical data. Minerals, 13(4), 471.

Rahimi, N., Niroomand, S., Lotfi, M., & Rahimi Shahid, M. (2022). Geology, mineralization, alteration and fluid inclusion studies of the Janja porphyry Cu-Mo deposit, Sistan Suture Zone, SE Iran. Scientific Quarterly Journal of Geosciences, 32(3), 13-30.

Reimann, C., Filzmoser, P., Garrett, R., & Dutter, R. (2011). Statistical data analysis explained: applied environmental statistics with R. John Wiley & Sons.

Saadati, H., Afzal, P., Torshizian, H., & Solgi, A. (2020). Geochemical exploration for lithium in NE Iran using the geochemical mapping prospectivity index, staged factor analysis, and a fractal model. Geochemistry: Exploration, Environment, Analysis, 20(4), 461-472.

Sadeghi, B., Zhao, H., & Holzheid, A. (2021). Preface: Mineral exploration: a journey from fieldwork, to laboratory work, computational modelling and mineral processing. Chemie der Erde/Geochemistry, 81(4), 125825.

Saremi, M., Agha Seyyed Mirzabozorg, S. A., Maghsoudi, A., Abedi, M., & DehghanNiri, R. (2025). Cu-bearing signatures from multi-element geochemical data, a correct strategy to implement a Convolutional Autoencoder Algorithm. International Journal of Mining and Geo-Engineering, 59(1), 1-10.

Saremi, M., Hoseinzade, Z., Mirzabozorg, S. A. A. S., Pour, A. B., Zoheir, B., & Almasi, A. (2024). Integrated remote sensing and geochemical studies for enhanced prospectivity mapping of porphyry copper deposits: A case study from the Pariz district, Urmia-Dokhtar metallogenic belt, southern Iran. Remote Sensing Applications: Society and Environment, 36, 101343.

Saremi, M., Maghsoudi, A., Hajihosseinlou, M., & Ghezelbash, R. (2024). A hybrid framework for detection of multivariate porphyry Cu signatures and anomaly enhancement: Incorporation of SFA, GMPI, and Grey Wolf Optimization. Geochemistry, 84(4), 126207.

Saremi, M., Yousefi, M., & Yousefi, S. (2023). Separation of geochemical anomalies related to hydrothermal copper mineralization using staged factor analysis in Feizabad geological map. Journal of Analytical and Numerical Methods in Mining Engineering, 14(38), 35-44.

Shah, S. T. H., Khan, N. G., Abbasi, M. I. H., Tabassum, K., & Shah, S. K. W. (2020). The Mineralization and structural geology of the porphyry copper deposits of Pakistan. Nepal Journal of Science and Technology, 19(2), 130-136.

Shahbazi, S., Ghaderi, M., & Afzal, P. (2021). Prognosis of of gold mineralization phases by multifractal modeling in the Zehabad epithermal deposit, NW Iran. Iranian Journal of Earth Sciences, 13(1), 31-40.

Shahrestani, S., & Mokhtari, A. R. (2017a). Dilution correction equation revisited: The impact of stream slope, relief ratio and area size of basin on geochemical anomalies. Journal of African Earth Sciences, 128, 16-26.

Shahrestani, S., & Mokhtari, A. R. (2017b). Improved detection of anomalous catchment basins by incorporating drainage density in dilution correction of geochemical residuals. Geochemistry: Exploration, Environment, Analysis, 17(3), 194-203.

Shahrestani, S., Mokhtari, A. R., & Alipour-Asll, M. (2019). Assessment of estimated bedrock and stream sediment geochemical backgrounds in catchment basin analysis. Natural resources research, 28, 1071-1087.

Shahrestani, S., Mokhtari, A. R., Carranza, E. J. M., & Hosseini-Dinani, H. (2019). Comparison of efficiency of techniques for delineating uni-element anomalies from stream sediment geochemical landscapes. Journal of Geochemical Exploration, 197, 184-198.

Siddiqui, R. H., Aftab, S. M., & Chaudhry, A. H. (2018). Hydrothermal Alteration in Porphyry Cu-Mo-Au Mineralizations of the Chagai Arc, Balochistan, Pakistan. IOP Conference Series: Materials Science and Engineering,

Siddiqui, R. H., Jan, M. Q., Khan, M. A., Kakar, M. I., & Foden, J. D. (2017). Petrogenesis of the Late Cretaceous tholeiitic volcanism and Oceanic Island arc affinity of the Chagai arc, western Pakistan. Acta Geologica Sinica-English Edition, 91(4), 1248-1263.

Sillitoe, R. H. (2010). Porphyry copper systems. Economic geology, 105(1), 3-41.

Spadoni, M. (2006). Geochemical mapping using a geomorphologic approach based on catchments. Journal of Geochemical Exploration, 90(3), 183-196.

Tazikeh, H., Khormali, F., Amini, A., & Motlagh, M. B. (2018). Geochemistry of soils derived from selected sedimentary parent rocks in Kopet Dagh, North East Iran. Journal of Geochemical Exploration, 194, 52-70.

Thiombane, M., Martín-Fernández, J.-A., Albanese, S., Lima, A., Doherty, A., & De Vivo, B. (2018). Exploratory analysis of multi-element geochemical patterns in soil from the Sarno River Basin (Campania region, southern Italy) through compositional data analysis (CODA). Journal of Geochemical Exploration, 195, 110-120.

Tolosana-Delgado, R., & Van den Boogaart, K. (2013). Joint consistent mapping of high-dimensional geochemical surveys. Mathematical Geosciences, 45, 983-1004.

Wang, J., & Zuo, R. (2024). Uncertainty quantification in geochemical mapping: A review and recommendations. Geochemistry, Geophysics, Geosystems, 25(3), e2023GC011301.

Wang, J., Zuo, R., & Caers, J. (2017). Discovering geochemical patterns by factor-based cluster analysis. Journal of Geochemical Exploration, 181, 106-115.

Wang, M., Wan, Y., Ye, Z., & Lai, X. (2017). Remote sensing image classification based on the optimal support vector machine and modified binary coded ant colony optimization algorithm. Information Sciences, 402, 50-68.

Wang, Z., Zhou, C., & Qin, H. (2020). Detection of hydrothermal alteration zones using ASTER data in Nimu porphyry copper deposit, south Tibet, China. Advances in Space Research, 65(7), 1818-1830.

Yousefi, M., & Carranza, E. J. M. (2015). Fuzzification of continuous-value spatial evidence for mineral prospectivity mapping. Computers & geosciences, 74, 97-109.

Yousefi, M., & Carranza, E. J. M. (2017). Union score and fuzzy logic mineral prospectivity mapping

using discretized and continuous spatial evidence values. Journal of African Earth Sciences, 128, 47-60.

Yousefi, M., Carranza, E. J. M., & Kamkar-Rouhani, A. (2013). Weighted drainage catchment basin mapping of geochemical anomalies using stream sediment data for mineral potential modeling. Journal of Geochemical Exploration, 128, 88-96.

Yousefi, M., Kamkar-Rouhani, A., & Carranza, E. J. M. (2012). Geochemical mineralization probability index (GMPI): a new approach to generate enhanced stream sediment geochemical evidential map for increasing probability of success in mineral potential mapping. Journal of Geochemical Exploration, 115, 24-35.

Yousefi, M., Kamkar-Rouhani, A., & Carranza, E. J. M. (2014). Application of staged factor analysis and logistic function to create a fuzzy stream sediment geochemical evidence layer for mineral prospectivity mapping. Geochemistry: Exploration, Environment, Analysis, 14(1), 45-58.

Yousefi, M., Kreuzer, O. P., Nykänen, V., & Hronsky, J. M. (2019). Exploration information systems–A proposal for the future use of GIS in mineral exploration targeting. Ore Geology Reviews, 111, 103005.

Zhang, J., Khalil, Y. S., Li, T., Wang, X., Guo, W., Wang, L., Hong, J., & Zhang, H. (2024). Source, distribution patterns and resources potential of selenium in soil of north Pakistan: Revealed by a national-scale geochemical mapping. Journal of Geochemical Exploration, 261, 107470.

Zuo, R. (2017). Machine learning of mineralization-related geochemical anomalies: A review of potential methods. Natural resources research, 26, 457-464.

Zuo, R., Kreuzer, O. P., Wang, J., Xiong, Y., Zhang, Z., & Wang, Z. (2021). Uncertainties in GIS-based mineral prospectivity mapping: Key types, potential impacts and possible solutions. Natural resources research, 30, 3059-3079.

Zuo, R., Xia, Q., & Zhang, D. (2013). A comparison study of the C–A and S–A models with singularity analysis to identify geochemical anomalies in covered areas. Applied geochemistry, 33, 165-172.

Zürcher, L., Bookstrom, A. A., Hammarstrom, J. M., Mars, J. C., Ludington, S., Zientek, M. L., Dunlap, P., & Wallis, J. (2019). Tectono-magmatic evolution of porphyry belts in the central Tethys region of Turkey, the Caucasus, Iran, western Pakistan, and southern Afghanistan. Ore Geology Reviews, 111, 102849.